九州大学学術情報リポジトリ
Kyushu University Institutional Repository

Integrated Workflow in 3D Geological Model Construction for Evaluation of CO2 Storage Capacity of a Fractured Basement Reservoir in Cuu Long Basin, Vietnam

Thanh, Hung Vo
Resources Production and Safety Engineering Laboratory, Department of Earth Resources Engineering, Graduate school of Engineering, Kyushu University

Sugai, Yuichi
Resources Production and Safety Engineering Laboratory, Department of Earth Resources Engineering, Faculty of Engineering, Kyushu University

Nguele, Ronald
Resources Production and Safety Engineering Laboratory, Department of Earth Resources Engineering, Faculty of Engineering, Kyushu University

Sasaki, Kyuro
Resources Production and Safety Engineering Laboratory, Department of Earth Resources Engineering, Faculty of Engineering, Kyushu University

https://hdl.handle.net/2324/4354919

出版情報：International Journal of Greenhouse Gas Control. 90, pp.102826-, 2019-11-01. Elsevier
バージョン：
権利関係：

KYUSHU UNIVERSITY

Integrated Workflow in 3D Geological Model Construction for Evaluation of CO_2 Storage Capacity of a Fractured Basement Reservoir in Cuu Long Basin, Vietnam

Hung Vo Thanh[1*, ID], Yuichi Sugai[1], Ronald Nguele[1] and Kyuro Sasaki[1]

[1]Resources Production and Safety Engineering Laboratory, Department of Earth Resources Engineering, Faculty of Engineering, Kyushu University, 744 Motooka Nishi-ku, Fukuoka 819-0395, Japan

[*]Corresponding author: vothanhhung198090@gmail.com

ORCID: 0000-0002-7094-9380

Abstract

Carbon dioxide (CO_2) capture, utilization, and storage (CCUS) have been proposed as a possible technique to mitigate climate change. In this vein, CO_2 storage through enhanced oil recovery (EOR) in depleted hydrocarbon reservoirs is touted as a most effective approach because it synergistically increases oil production and enables permanent sequestration into the reservoirs. However, the construction of a reasonable 3D geological model for this storage reservoir is a major challenge. Thus, this study presents an efficient workflow for constructing an accurate geological model for the evaluation of CO_2 storage capacity in a fractured basement reservoir in the Cuu Long Basin, Vietnam. Artificial neural network (ANN) has been used to predict porosity and permeability values through seismic attributes and well log data. The predicted values were selected using high correlation factors with well log data. Subsequently, the Sequential Gaussian Simulation and co-kriging methods were applied to generate a 3D static geological model by using azimuth and dip parameters. Finally, drill stem test matching was performed to validate the accuracy of the porosity and permeability models through dynamic simulation. A validation 3D reservoir model, which integrates geophysical, geological, and engineering data from fractured basement formation in Cuu Long Basin, was further constructed to calculate theoretical CO_2 storage capacity. As a result, the calculated storage capacity for the fractured basement reservoir ranged from 7.02 to 99.5 million metric tons. These estimated results demonstrate that fractured basement reservoir has a combined potential for CO_2 storage and EOR in the Cuu Long Basin.

Keywords: Artificial neural networks, CO_2 storage capacity calculation, Integrated 3D geological model, Fractured basement reservoir, Cuu Long Basin

1. INTRODUCTION

Carbon dioxide (CO_2) capture, utilization, and storage (CCUS) have been touted as a common approach to mitigate greenhouse gas effect and climate change (Bachu, 2000; Hitchon et al., 1999; IPCC, 2005). CO_2 may be stored in deep saline aquifers, depleted hydrocarbon reservoirs, and/or depleted fractured shale formations (Bachu, 2002; Edwards et al., 2015). Among these plausible sequestration zones, oil and gas depleted reservoirs have been the most practical sites to store CO_2 because these reservoirs have available geological data from the history of exploration and production (Zhao and Liao 2012; Dai et al. 2017; Van't Veld et al. 2013).

Moreover, injecting CO_2 into an oil-bearing formation has the potential to enhance oil recovery. This technique, hereinafter referred to as CO_2-EOR, coupled/associated with the gas storage can defray the cost of sequestration (Hill et al. 2013; Ettehadtavakkol et al. 2014; Ampomah et al. 2017; Lee et al. 2019). The CO_2–EOR and its storage potential have been investigated by many projects worldwide (Bachu, 2018; Choi et al., 2013; Nguyen-Trinh and Ha-Duong, 2015; Pham and Halland, 2017; Wei et al., 2015).

The Asian Development Bank (ADB, 2012) proposed that the 14 oil and gas fields offshore Cuu Long Basin can provide 900 megatons of CO_2 storage capacity. In this regard, a collaboration between Petro Vietnam and Mitsubishi Heavy Industries examined the feasibility of CO_2–EOR in the White Tiger oil field (Imai and Reeves, 2004). Approximately, 7.4 million tons per year of CO_2 was injected, which led to an increment of oil recovery to 50 thousand barrels of crude oil per day (Imai and Reeves, 2004).

Rather than focusing on CO_2 storage, the project discussed above aimed at improving the oil recovery. It further reported a decline in oil production subsequent to the dissolution CO_2 in the oil as well as the leakage of CO_2 from fault or fracture in the reservoir (Ha-Duong and Nguyen-Trinh, 2017). Another drawback, further believed to be a plausible reason for the decline in sequestered CO_2, was the complicated reservoir geological model in the White Tiger field. This is to say that there is a need for reliable 3D geological model construction in order to better and/or improve both CO_2 storage and CO_2-EOR process.

Unlike sandstone reservoirs, to which conventional workflow can be applied to construct 3D geological models, a fractured basement reservoir, which is the case for Cuu Long Basin, could not be easily simulated based on core and well logs. This was so because fractures and faults

represented for the matrix and its petrophysical properties. In addition, the seismic data could not distribute the small fractures. Thus, artificial neural network (ANN) and geostatistic approaches have been applied to distribute the whole porosity and permeability properties for fracture basement reservoir (Nguyen et al. 2011).

ANN is an Artificial Intelligence tool applied in many fields and for varying applications. In petroleum engineering, ANN has been adapted in many studies such as: predicting porosity and permeability of petroleum reservoirs (Ahmadi et al. 2014); estimating the dew point pressure and condensate-to-gas ratio in condensate gas reservoirs (Ahmadi and Ebadi 2014; Ahmadi et al. 2014); predicting the asphalting precipitation (Ahmadi and Shadizadeh 2012; Ahmadi 2011) among others. Recently, ANN has been used to predict the solubility of CO_2 in brines and CO_2 storage efficiency (Ahmadi and Ahmadi, 2016; Kim et al., 2017). These authors demonstrated the effectiveness of the ANN method as predictive models for the earlier stated objectives.

On the other hand, geostatistics approaches (i.e., Sequential Gaussian Simulation (SGS) and co-kriging) are efficient methods to distribute the 3D petrophysical reservoirs model (Esmaeilzadeh et al. 2013). In recent years, some studies have demonstrated the effectiveness of geostatistical methods to construct the realistic geological model for the CO_2 storage application in a fluvial sandstone reservoir (Nguyen et al. 2017; Vo Thanh et al. 2019).

Nguyen et al. (2017) used SGS for 3D petrophysical modeling to investigate the CO_2 plume dynamic in the deep saline aquifer. Vo Thanh et al. (2019) adapted SGS and co-kriging for the new geological modeling workflow to enhance CO_2 storage assessment in the meandering fluvial reservoir.

Thus, based on advantages of ANN, SGS and co-kriging method, this work proposed an integrated workflow to build accurate geological models for fractured basement reservoirs. This procedure is intended to solve the problem of limited good data and complex structure in fractured reservoirs. From a broader aspect, combining both ANN, Sequential Gaussian Simulation and co-kriging is expected to improve the calculation of the theoretical storage capacity of CO_2 in fractured basement reservoir in Cuu Long Basin, Vietnam. Because this study aims to calculate theoretical CO_2 storage capacity in a fractured basement reservoir in Cuu Long Basin, Vietnam. Moreover, our work aims to establish and validate an integrated workflow to evaluate CO_2 storage capacity that can be applied in other fractured basement

reservoirs. To the best of our knowledge, this study is the first to be conducted on geological modeling in fractured basement reservoirs to evaluate potential CO_2 storage.

In sum, this study mainly aims to achieve the following objectives:

- to predict porosity and permeability values through the ANN method,
- to distribute porosity and permeability in the 3D model through co-kriging approach,
- to validate the accuracy of reservoir model through drill stem test (DST) matching, and
- to estimate theoretical CO_2 storage capacity.

2. GEOLOGICAL BACKGROUND

Cuu Long Basin constitutes an Early Tertiary rift basin located off the southeast coast of Vietnam extending from latitude 9° to 11° north and covering an area of approximately 25,000 km². This basin is a rift-type Early Cenozoic subsided trough. The basin is found on the pre-Cenozoic active regressive continental crust and filled with Late Cenozoic passive continental margin sediments (Hung and Le, 2004).

The tectonic evolution of Cuu Long Basin can be divided into several main stages including (Schmidt et al., 2019):

- Late Cretaceous–Eocene: pre-rift uplift.
- Late Eocene–Oligocene: main rifting phase. This phase led to the development of main structural features within the basins, following extensional and transtensional deformations.
- Early Middle Miocene: regional subsidence. This phase was marked by a change from typically fault-controlled subsidence to a thermally controlled, high-rate subsidence.
- Late Miocene: partial inversion. During this stage, the entire area became dominated by compression, which, in combination with the dextral strike-slip fault system in east offshore Vietnam, probably generated basin uplift/partial inversion.
- Pliocene–Pleistocene: regional subsidence. Diverse tectonic activity, from low to moderate amplitude differential uplift, acted across the basins in the area.

Nam Vang (NV) field is located along the northwestern margin of the Cuu Long Basin, which is located offshore of southern Vietnam. The granite fractured basement is the main reservoir in the NV field. This basement is composed of granite and granodiorite, which are locally metamorphic and volcanic and can be divided into upper and lower zones. The upper zone consists of weathered granitoids with thickness varying from a few meters to tens of

meters. The lower zone is fresh fractured granite, and these fractures are partly filled mainly by secondary calcite and zeolite. Some of the dyke rocks are also cut granitoids (Cuong and Warren, 2009).

The other reservoir targets are in Oligocene sandstones of Tra Tan formation and the Lower Miocene fluvial sandstone of Bach Ho formation. Oil and gas have been explored in the sandstone of E, C, BI.1, and BI.2 sequences in the NV field (**Figure 1**). The good source rock in the NV field is lacustrine shale of D and E sequences with a large amount of total organic carbon and hydrocarbon index values. These sequences also formed the seal for Oligocene sandstone and fractured granitoids basement reservoirs (Cuong and Warren, 2009; Hung and Le, 2004). The entire stratigraphic sequences of NV field are shown in **Figure 1.**

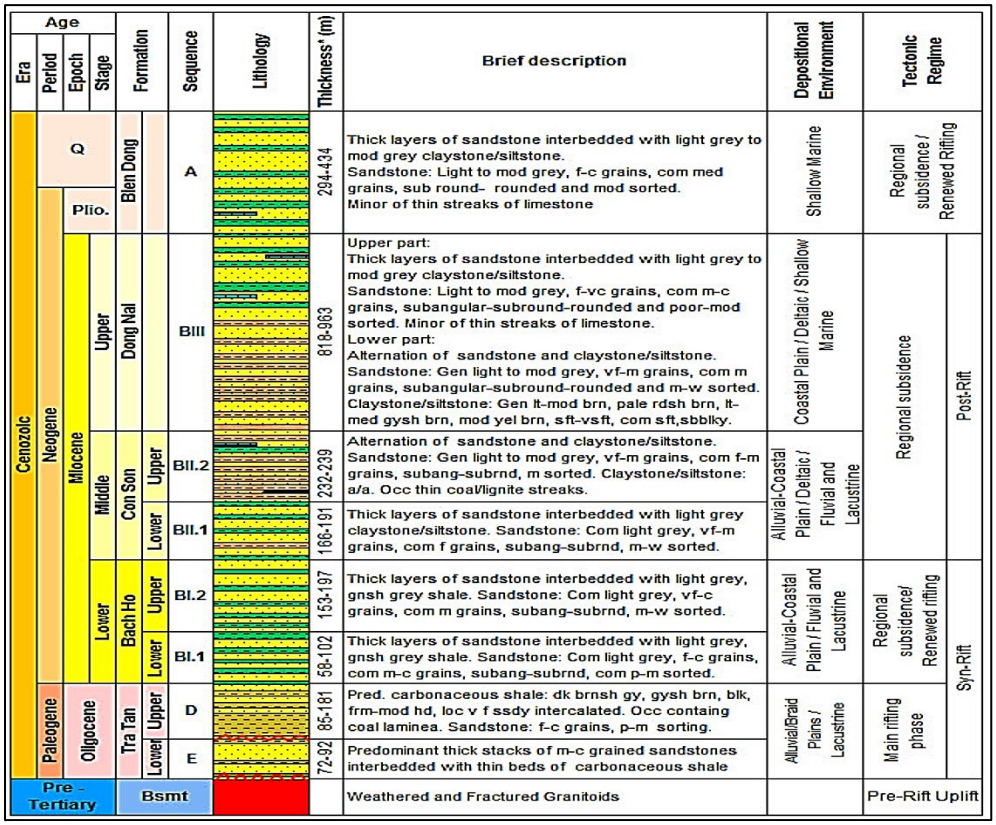

Figure 1. Stratigraphic column of NV field in Cuu Long Basin.

2.1. CO_2 sources

At normal standard conditions, CO_2 is a thermodynamically steady gas with a density of 1.872 kg/m^3, which is slightly heavier than air. CO_2 is in a supercritical state with temperatures higher than 31.1 °C and pressures higher than 7.38 MPa (critical point).

At supercritical conditions, the properties of CO_2 are absolutely different from those of CO_2 in either liquid or gaseous phase, which acts in a manner similar to gas by occupying all the available volume to increase the mass (Bachu, 2008, 2000; Holloway and Savage, 1993).

The CCUS potential in Vietnam was proposed by ADB in 2012. In this investigation, the anthropogenic sources could have amounted to 53 million tons of CO_2 emissions which identifies as a potential candidate for carbon capture and storage (CCS) (APEC, 2014). These sources are future natural gas combined cycle and subcritical coal-fired power plants (ADB, 2012; APEC, 2014). In the light of CCS activities in Vietnam, the Phu My Fertilizer Plant was established as a CO_2 capture facility near Vung Tau City, Vietnam. It was proposed that CO_2 injection equipment, oil and gas separator, and recycled CO_2 plant will be located 150 km southeast of Vung Tau City in the study area (**Figure 2**). CO_2 injection sites are to be located near the previous CCS sites, such as Rang Dong field. With this, the risks of CO_2 transportation source to sink could be reduced through the connection from the storage site to the other fields, as investigated for the CCS project.

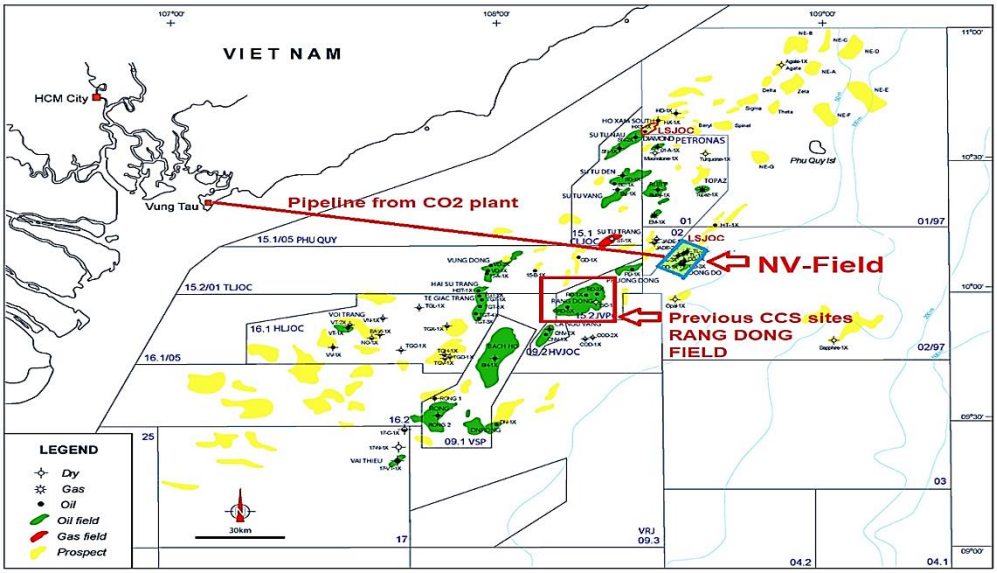

Figure 2. NV field view showing a fractured basement reservoir as modelled in this study. The blue polygon indicates the study area. The red line shows distance from the CO_2 power plant to the injection site.

2.2. Available data

The database established in this study includes seismic interpretation data, well log data, formation micro imager (FMI) analysis, Drill Stem Test (DST) data, and other geological information. The seismic interpretation includes top and base surfaces and fault system (**Figures 3a and 3b**). Well logs from three wells, namely, NV-1X, NV-2X, and NV-3X, are used. These wells have two well log parameters, namely, porosity and permeability (**Figure 3c**). In the study area, three wells have FMI data (**Figure 3d**). The result of FMI interpretation is key to define the dip, strike, and the azimuth of the fractured or fault zones.

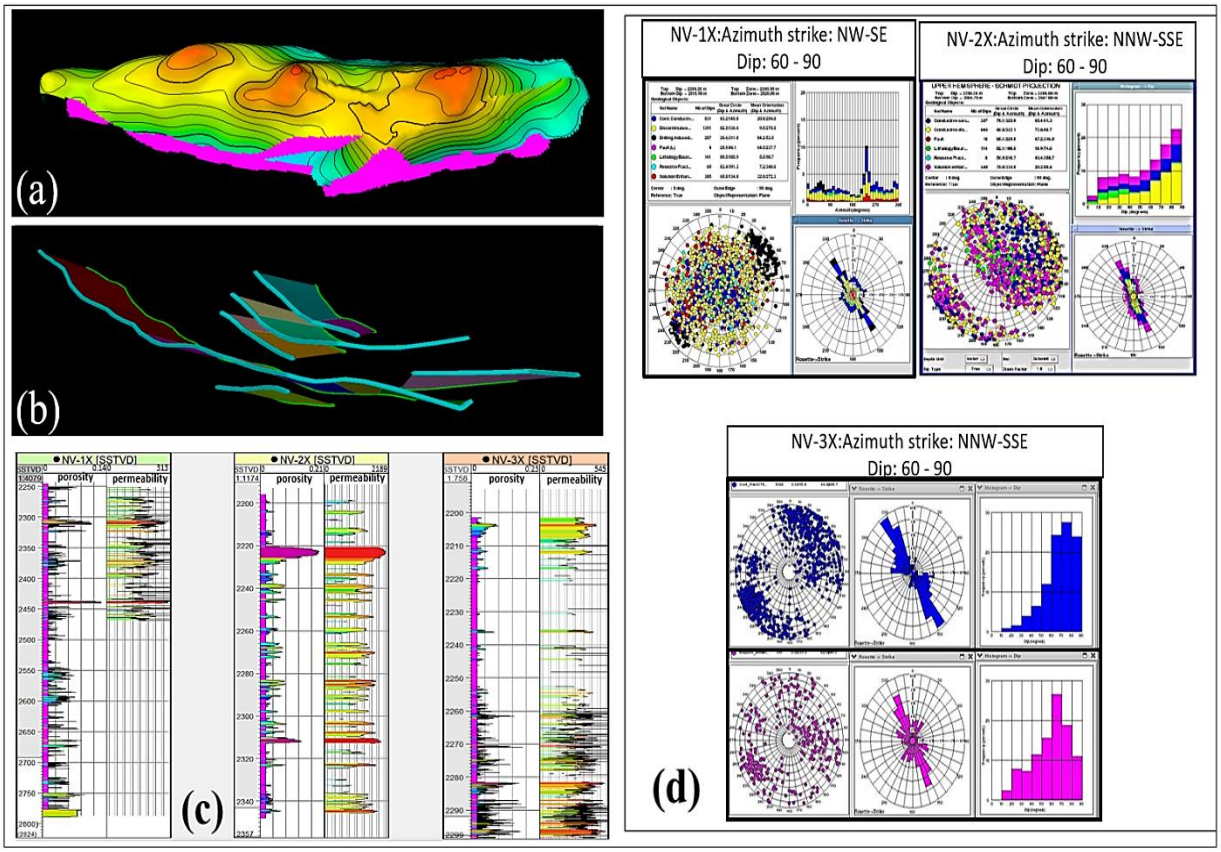

Figure 3. Illustration of data used in this study: (a) seismic horizon from seismic interpretation, (b) fault system in fractured basement reservoirs, (c) well log data including porosity and permeability values, and (d) FMI interpretation to obtain azimuth and dip parameters

A DST was performed in the NV-2X and NV-3X wells to evaluate the reservoir characteristics. Bottom-hole pressure measurements were conducted through the DST process. These measurements are used in history matching to verify the accuracy of the geological model. The DST analysis results are summarized in **Table 1**. During DST operations, surface samples from the fractured basement reservoirs were considered and analyzed using traditional pressure volume temperature (PVT) analysis. Some of the key properties acquired, including bubble point pressure (P_b**)**, gas-oil ratio (R_s**)**, formation volume factor (FVF), oil viscosity, and produced oil gravity, are listed in **Table 2**. The oil-water permeability curves used in the simulation were obtained from special core analysis performed on the cores from Cuu Long Basin.

Table 1. Summary of the DST data in fracture basement reservoir

Properties	NV-2X	NV-3X
	DST#1 2280-2577m	DST#1 2352-3690 m
Flow Period	Main Build-up	Main Build-up
k (mD)	167	81.92
Skin Factor	2.7	-1.92
P_i (psia) at gauge Depth (mMDDF)	3147@2184.78	3218.3 @2341

Table 2. PVT analysis from NV-2X well

Properties	NV-2X - DST#1
Gravity (API 60^{o}F)	24.5
P_b (psia)	1,130
R_s (scf/stb)	183
FVF @ Pres (rb/stb)	1.128
Viscosity @ Pb (cP)	6.924

3. METHODOLOGY

3.1.Theory

3.1.1. Artificial Neural Network (ANN)

ANN is a computational tool, which helps automatically identify the relationship between multiple known parameters and a single unknown parameter. The behavior of a neural network is defined by the way that their individually computed elements are connected and by the strength of those connections, or weights. Weights are automatically adjusted by training the network in accordance with a specified learning rule until it properly performs the desired task (Ahmadi, 2015). Basically, ANN applications have two stages: the training stage, where the ANN learns the hidden relationship of data while the predicting stage of ANN was used to predict new outputs from input data not used during the training stage (Ruiz- Serna et al., 2019).

Also, ANN can be roughly categorized into two types in terms of their learning features: supervised and unsupervised (Anderson and McNeill, 1992). This research is used supervised ANN model, which is a toolbox in Petrel that takes multiple inputs and returns one or several outputs from trial and error algorithm (Petrel, 2017). These inputs included seismic attributes and well log values. Each input was multiplied by a weight, the result was then summed and passed through a nonlinear function to produce the output (Darabi et al., 2010; Du et al., 2003; Iturrarán-Viveros and Parra, 2014; Mahdavi and Kharrat, 2009; Nikravesh, 1998). Figure 4 depicts the basic structure of the ANN model as used in this study.

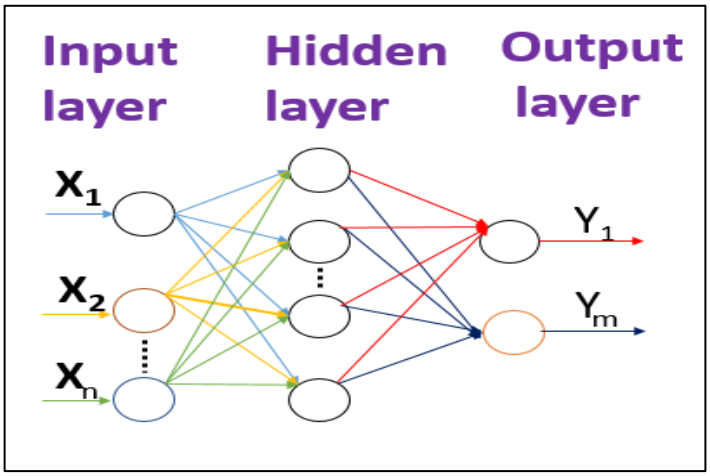

Figure 4. Basic ANN structure. In this illustration, there are three input attributes, four neurons in the hidden layer, and two log samples in the output layer

3.1.2. Sequential Gaussian Simulation (SGS) and Co-kriging

SGS is a stochastic modeling technique to generate random fields of continuous variables such as porosity and permeability (Pyrcz and Deutsch, 2014). Also, this algorithm is more efficient than Truncated Gaussian Simulation because it does not consider the orderly transition between facies types (Al-mudhafar, 2018). Hence, its utilization in this study.

The procedure of Sequential Gaussian Simulation can be expressed as follows (Pyrcz and Deutsch, 2014): (1) changing all the original selected data into Gaussian population by: Mean equal to 0 and Standard Deviation equal to 1 through the normal score transformation (Z-distribution); (2) generating the variogram for the selected data; (3) selecting randomly the location of evaluation from the seed number; (4) determining the variable values and the related error variance at that location via the co-kriging approach; (5) creating the local conditional cumulative distribution function for the variables at that location for random selecting the values using that function.

Also, in this study, the co-kriging approach was adapted to solve challenges of limited well data by integrating the predicted ANN values that have a good correlation with the primary well data (Esmaeilzadeh et al. 2013). This approach uses a correlation factor between primary and secondary data to calculate the distribution of the secondary variable at each point. The correlation factor can be a constant**,** surface or property and can be positive or negative values (Petrel, 2017).

Besides, the calculated correlation factor between the simulated primary variables and the secondary variables is often not equal to the input correlation. This is a hurdle associated with the SGS algorithm. But within the geological package (Petrel), there is a basic mechanism to overcome such a bias, named as the variance reduction factor. This value ranging from 0 to 1 can be selected by trial and error to overcome the bias (Petrel, 2017).

3.2.Workflow

In this study, 3D geological model procedures used in CO_2 storage capacity evaluation compromised: (1) building a structural model to display faults, zones, and layering of reservoirs; (2) predicting porosity and permeability models using ANN, (3) constructing a 3D petrophysical model through SGS and co-kriging to integrate the prediction models; (4) DST matching to validate the accuracy of the porosity and permeability models; and (5) evaluating the theoretical CO_2 storage capacity based on specific equations proposed by Bradshaw et al. (2005, 2007). **Figure 5** depicts the schematic of the modeling workflow in this study.

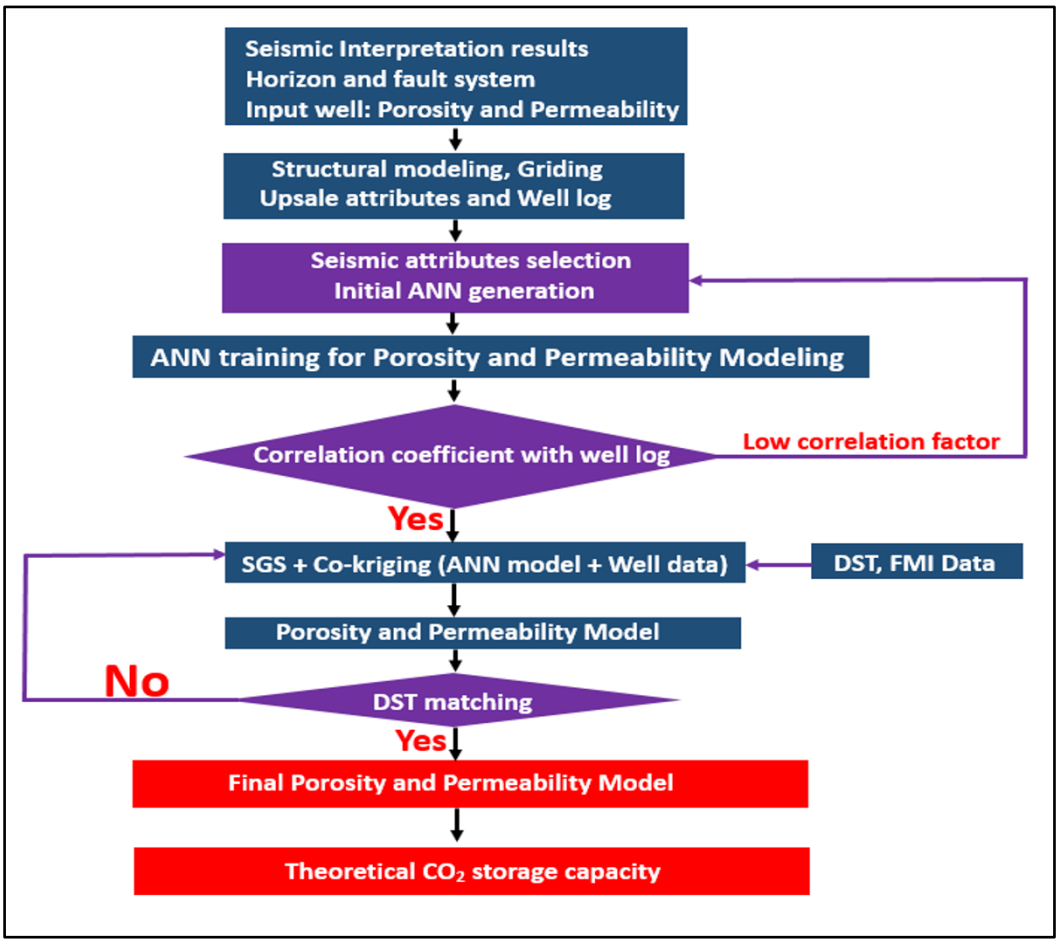

Figure 5. Schematic representation of the integrated workflow to estimate theoretical CO_2 storage capacity

The fault and seismic interpretations were used to construct the structural model, which provided the framework for the 3D petrophysical model. The petrophysical properties of conventional well logs in fractured basement reservoirs were difficult to

use in estimation. Thus, ANN was utilized to predict these properties to build the needed 3D model. The arithmetic average method was applied to upscale the porosity and permeability values from well logs to the grid. These values were also applied in the ANN training to obtain the predicted porosity and permeability models.

Then, a variogram of the upscaled porosity and permeability was used to illustrate a suitable model trend. Afterwards, SGS and co-kriging were combined to create 3D petrophysical models. The predicted models from ANNs were used as secondary variables in collocated co-kriging.

3.3. THREE-DIMENSIONAL GEOLOGICAL MODELING

3.3.1. Structural modeling

A 3D structural model is constructed on the base of a top surface, which is on top of the basement, and a base surface, which is a flat horizon at 2500 m. The fault system was generated from depth fault sticks. Subsequently, the pillar gridding was developed based on the skeleton framework. The skeleton is a grid consisting of a top, middle, and base skeleton grid. In fractured basement reservoirs, the grid has no layers, and only a set of pillars are given I and J increments, which are set to 25 by 25 m, respectively. The fault systems, modelled in this study, consisted of zig-zag type faults. Then, the vertical resolution of the 3D grid is defined using the 'make a zone' functional tool in Petrel.

The layering process was the final step in building the structural framework to define the thickness and orientation of the layers of the 3D grid. The "follow base" layering functionality was used to develop the grid model. The number of layers depends on cell thickness. In this study, a series of parameters of cell thickness (10, 20, 30, and 40 m, respectively) were tested.

The cell thickness affects the value of well log upscaling and the correlation coefficient between well and seismic data for further steps. Hence, optimizing the grid size during well log upscaling is necessary. Two well log parameters consisting of porosity permeability were (**Figure 3c**) used to scale up the model. The good correlation between seismic attributes and well porosity was indicated by the optimal grid cell with 20 m thickness (**Figure 6a**). Similarly, the permeability upscaling was also performed with similar grid cell thickness (**Figure 6b**). The total size of the grid cell was 25 × 25 × 20 m

after optimization (**Table 3**). The structural model of the fractured basement reservoirs is shown in **Figure 7.**

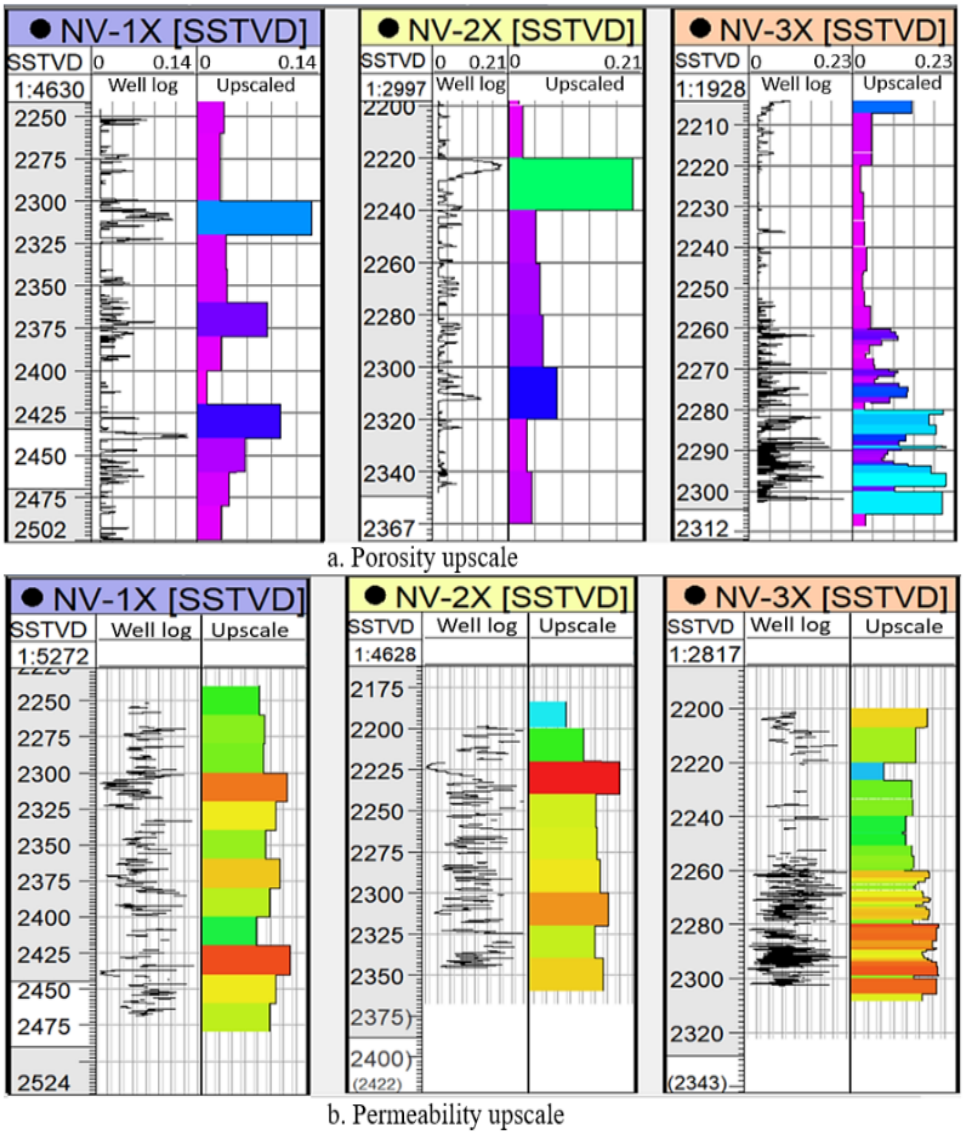

Figure 6. Upscaling porosity and permeability to define grid cell number for a structural model

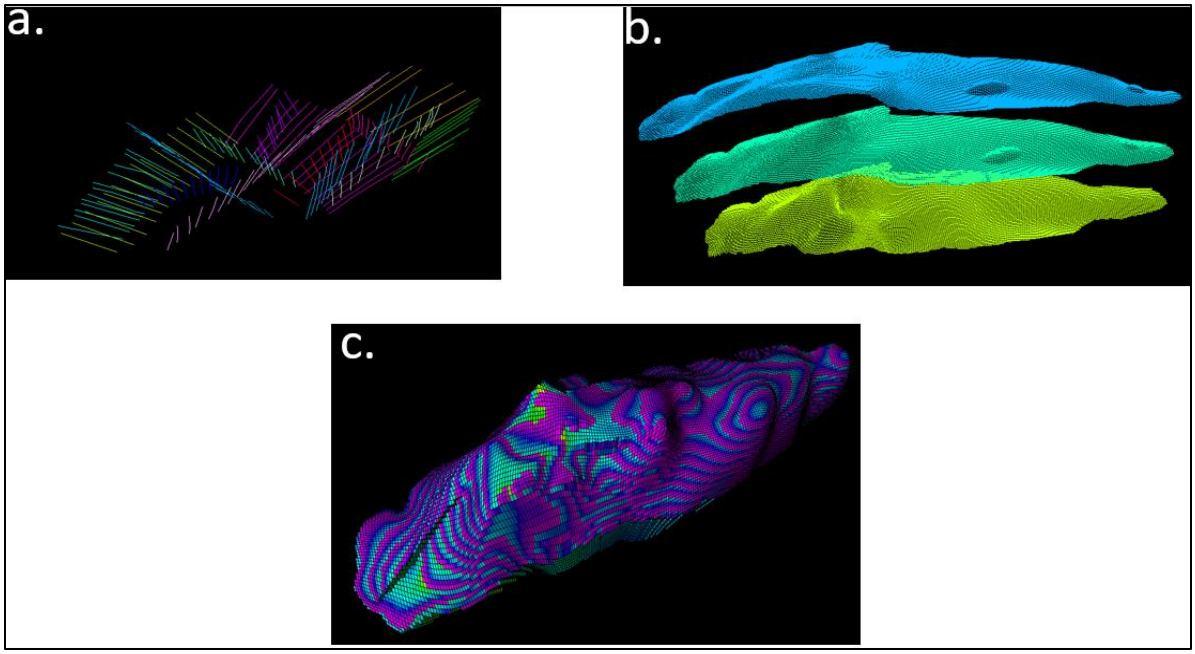

Figure 7. Structural modeling process for fractured basement reservoirs. (a) Develop fault system; (b) skeleton grid; (c) final structural model

Table 3. Optimizing the layer's size for structural modeling

Layer's size	Number of cells Porosity Upscale	Number of cells Permeability Upscale	Total cells
10m	117	116	771,120
20m	92	90	396,576
30m	77	76	264,384
40m	74	73	198,288

3.3.2. Petrophysical prediction models by ANNs

Porosity is a fundamental and crucial property in defining the storage capacity of fluids in reservoirs. Whereas, permeability is an important parameter to measure the ability of fluid flow in connected porous media. Therefore, the accuracy of porosity and permeability is essential in minimizing errors in reservoir characterization and geological modeling in the

hydrocarbon field. These parameters could be obtained from core interval and well log measurements in wells. Nonetheless, conventional geological workflows cannot distribute these petrophysical parameters properly due to the limited core data and conventional modeling. Thus, ANN is an excellent method to solve these nonlinear problems in the oil and gas industries. In this study, ANN is used to estimate the porosity and permeability from seismic attributes and well logs.

3.3.2.1.Generating seismic attributes

Seismic data were used in establishing the seismic attributes (**Figure 8a**). The attributes were further grouped according to four specific tasks, namely, signal processing method, complex trace, structural, and stratigraphic. Therefore, 20 seismic attributes were generated in this step following the specific tasks (**Figure 8b**). Then, all the established seismic attributes were sampled into the structural model by geometrical modeling module with arithmetic method from Petrel software. The generated seismic attributes were utilized for the ANN study to determine the good correlation between the predicted and well log petrophysical properties.

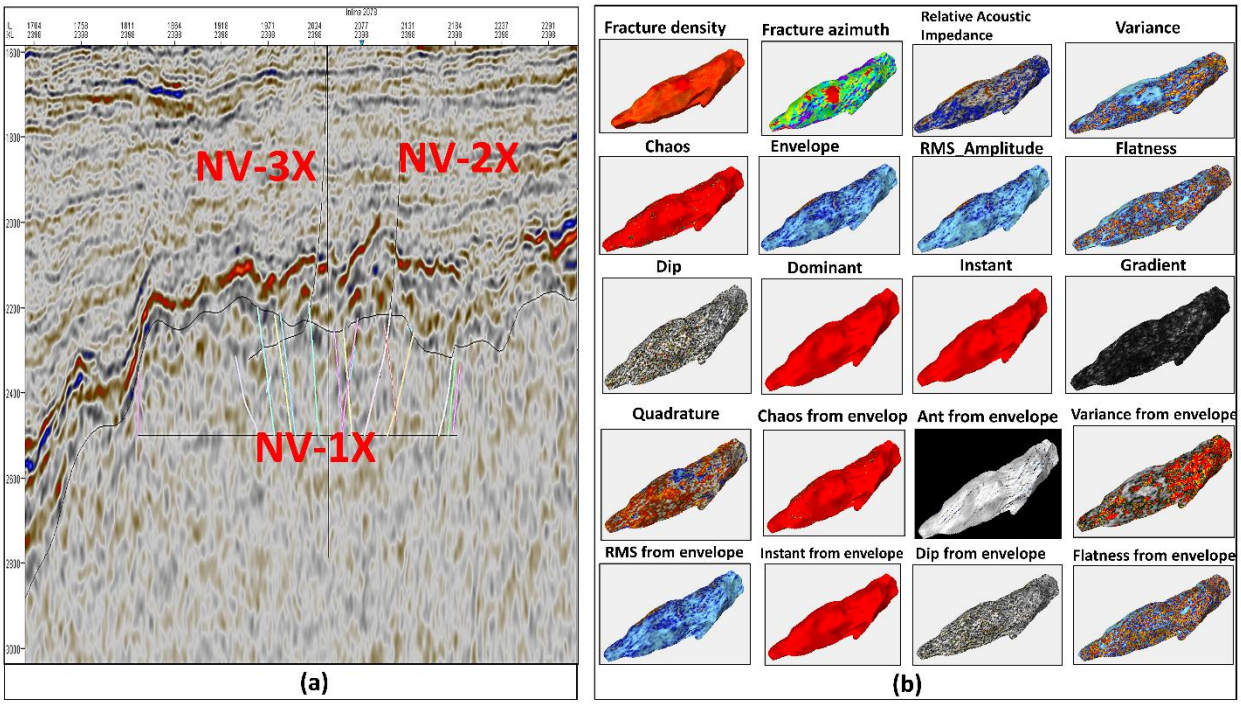

Figure 8. Seismic data for ANN training: (a) cross-section of seismic data along reservoir wells and (b) seismic attribute generation for the ANN process

3.3.2.2.Porosity and permeability establishment from ANN training

Figure 9a and 9b depict the workflow for establishing the porosity model through the ANN model. The ANN technique is applied to integrate selected seismic attributes with well porosity to predict the distribution of porosity in the fractured basement reservoirs. The 20 seismic attributes were used in generating several scenarios to rank the best group for the ANN training. Based on these scenarios, the correlation coefficient between the well and predicted porosities were later calculated to select the best probable scenario in predicting the porosity model.

The result of ranking the seismic attributes is presented in **Table 4.** Scenario 5 is the best scenario because it has the highest correlation coefficient (0.88) calculated at the well after propagation in 3D (**Figure 9c**).

Table 4. Ranking to select the best group seismic attributes for ANN prediction

Scenario	Seismic attributes	Correlation factor
1	Variance, Chaos, Dip Deviation, Ant-Tracking from Envelope, Fracture Density, Fracture Azimuth	0.46
2	Relative Acoustic Impedance (RAI), Variance, Dip Deviation, Chaos from Envelope, Ant-Tracking from Envelope, Fracture Density, and Fracture Azimuth	0.52
3	RAI, Variance, Chaos, Dip Deviation, Chaos from Envelope, Dip Deviation from Envelope, Fracture Density, Fracture Azimuth	0.66
4	RAI, Variance, Chaos, Dip Deviation, Quadrature, Ant-Tracking from Envelope, Dip Deviation from Envelope, Fracture Density, Fracture Azimuth	0.75
5	RAI, Variance, Chaos, Fracture Density, Fracture Azimuth, Envelope, Flatness, Instant from Envelope, Dip Deviation from Envelope, Flatness from Envelope	0.88

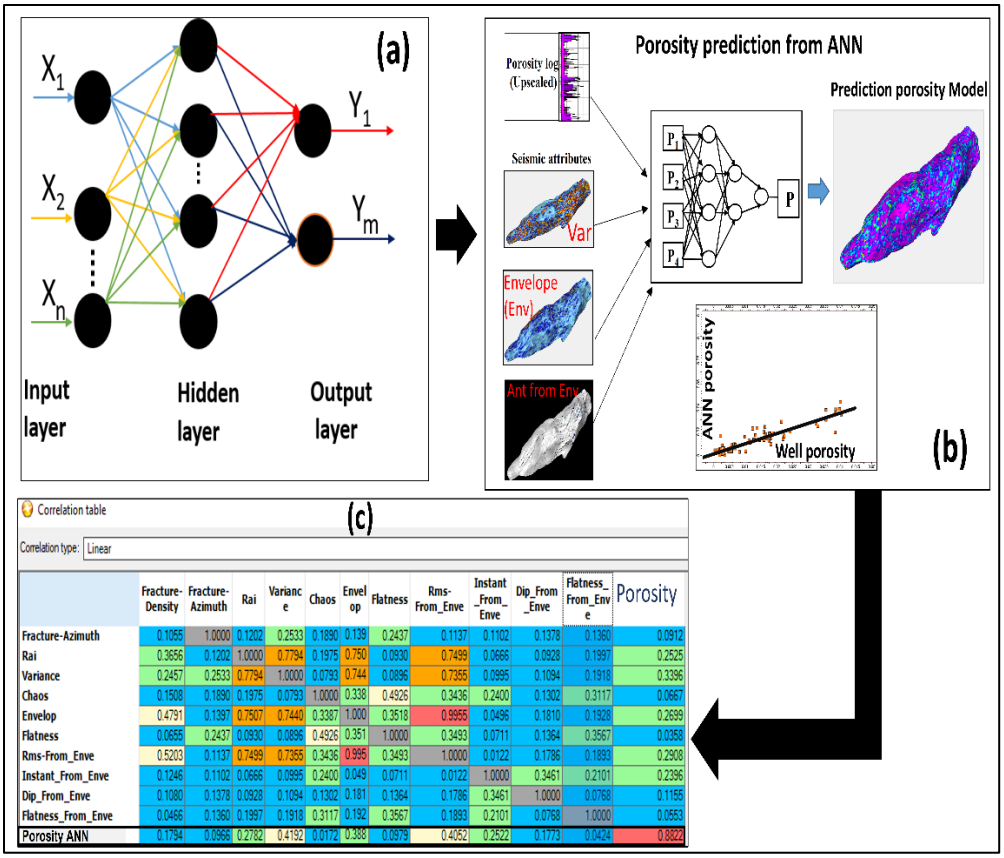

	Fracture-Density	Fracture-Azimuth	Rai	Variance	Chaos	Envelop	Flatness	Rms-From_Enve	Instant_From_Enve	Dip_From_Enve	Flatness_From_Enve	Porosity
Fracture-Azimuth	0.1055	1.0000	0.1202	0.2533	0.1890	0.139	0.2437	0.1137	0.1102	0.1378	0.1360	0.0912
Rai	0.3656	0.1202	1.0000	0.7794	0.1975	0.750	0.0930	0.7499	0.0666	0.0928	0.1997	0.2525
Variance	0.2457	0.2533	0.7794	1.0000	0.0793	0.744	0.0896	0.7355	0.0995	0.1094	0.1918	0.3396
Chaos	0.1508	0.1890	0.1975	0.0793	1.0000	0.338	0.4926	0.3436	0.2400	0.1302	0.3117	0.0667
Envelop	0.4791	0.1397	0.7507	0.7440	0.3387	1.000	0.3518	0.9955	0.0496	0.1810	0.1928	0.2699
Flatness	0.0655	0.2437	0.0930	0.0896	0.4926	0.351	1.0000	0.3493	0.0711	0.1364	0.3567	0.0358
Rms-From_Enve	0.5203	0.1137	0.7499	0.7355	0.3436	0.995	0.3493	1.0000	0.0122	0.1786	0.1893	0.2908
Instant_From_Enve	0.1246	0.1102	0.0666	0.0995	0.2400	0.049	0.0711	0.0122	1.0000	0.3461	0.2101	0.2396
Dip_From_Enve	0.1080	0.1378	0.0928	0.1094	0.1302	0.181	0.1364	0.1786	0.3461	1.0000	0.0768	0.1155
Flatness_From_Enve	0.0466	0.1360	0.1997	0.1918	0.3117	0.192	0.3567	0.1893	0.2101	0.0768	1.0000	0.0553
Porosity ANN	0.1794	0.0966	0.2782	0.4192	0.0172	0.388	0.0979	0.4052	0.2522	0.1773	0.0424	0.8822

Figure 9. Adoption of ANN structure to predict porosity values from upscale well log and seismic attributes: (a) structure of ANN model, (b) schematic of porosity prediction from ANN, and (c) correlation table of predicted and well log porosities

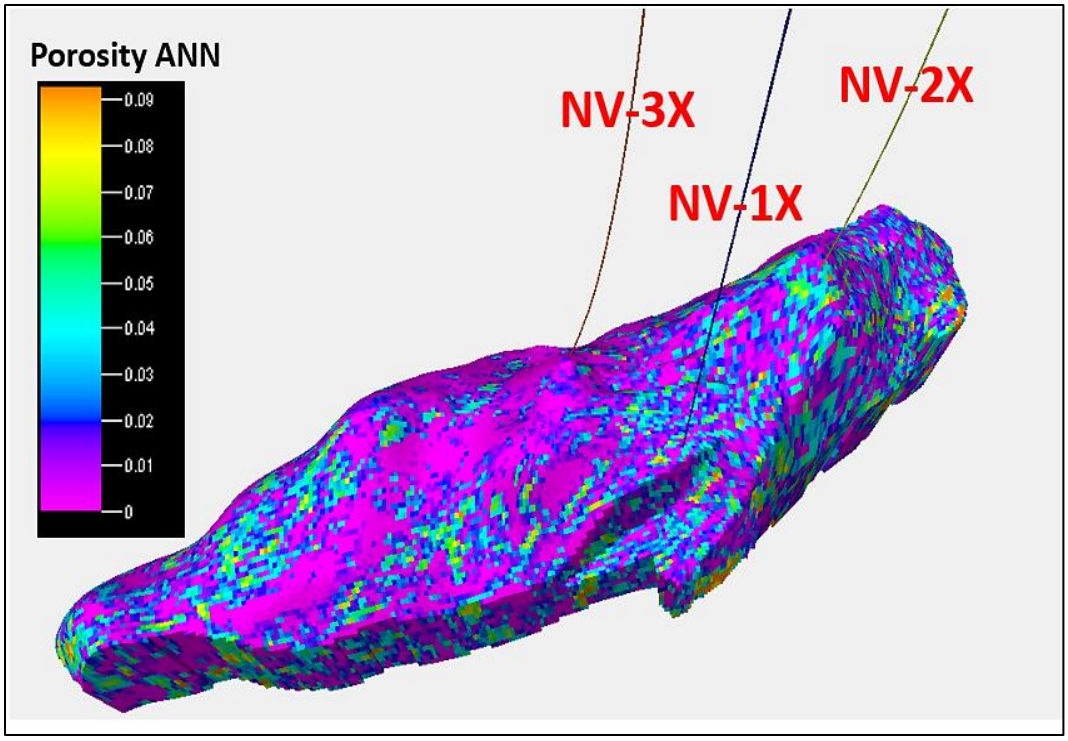

Figure 10. Distribution of porosity model from ANN

The result of ANN porosity is shown in **Figure 10**. The predicted porosity of each well from ANN is extracted to verify against the input well porosity. **Figure 11** depicts the visually checked and cross plot between ANN and well log porosities. The distribution of the predicted porosity is consistent with well porosity. The process of permeability prediction is similar to that of porosity, therefore, not elaborated. The result of the ANN permeability model is shown in **Figure 12**. The predicted permeability cube was extracted for comparison with the well permeability. The comparison indicates that the correlation factor is quite high to confirm the accuracy of the ANN permeability model (**Figure 13**). Through the validation between the predicted and well parameters, the result of the ANN porosity and permeability models were highly reliable for use in petrophysical modeling

.

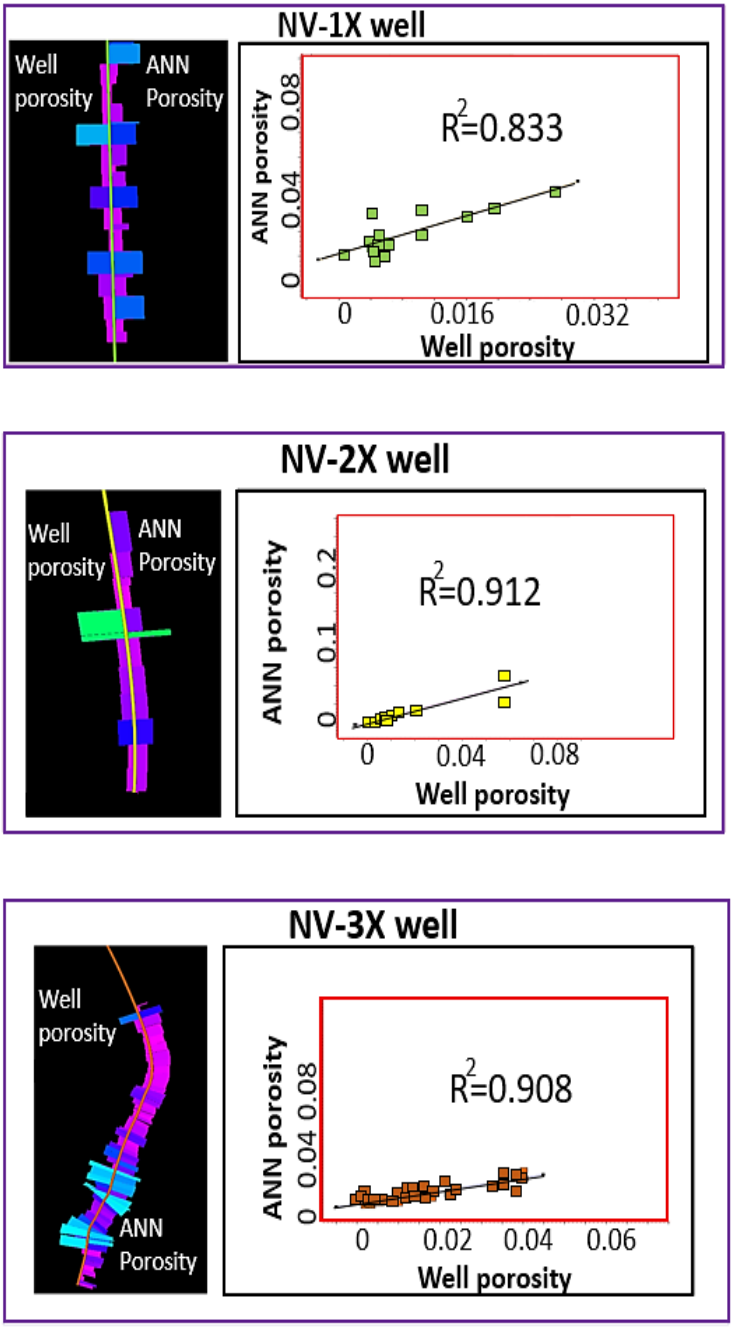

Figure 11. Cross-validation to check correlation factor between ANN and well log porosity values

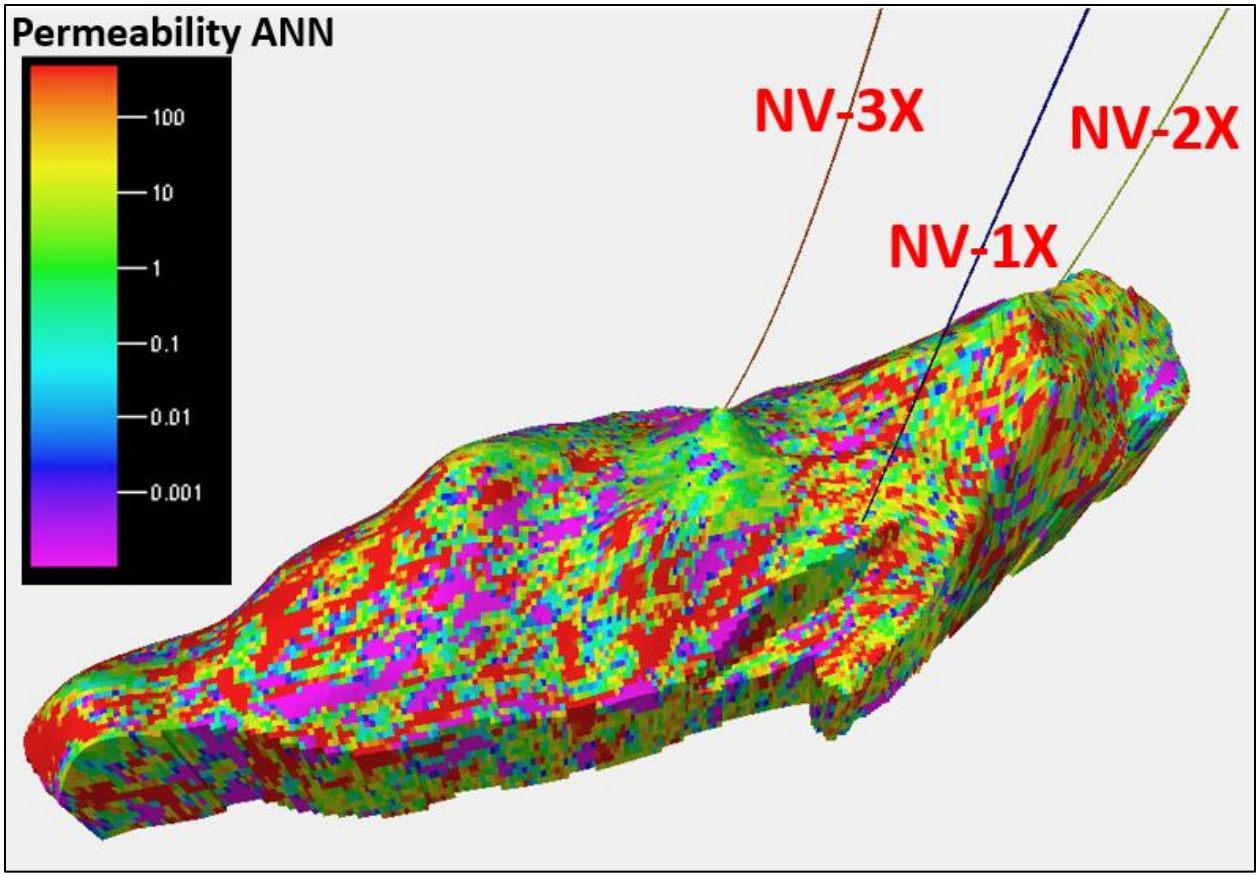

406

407 **Figure 12.** Distributed permeability model as predicted by ANN

408

409

410

411

412

413

414

415

416

417

418

419

420

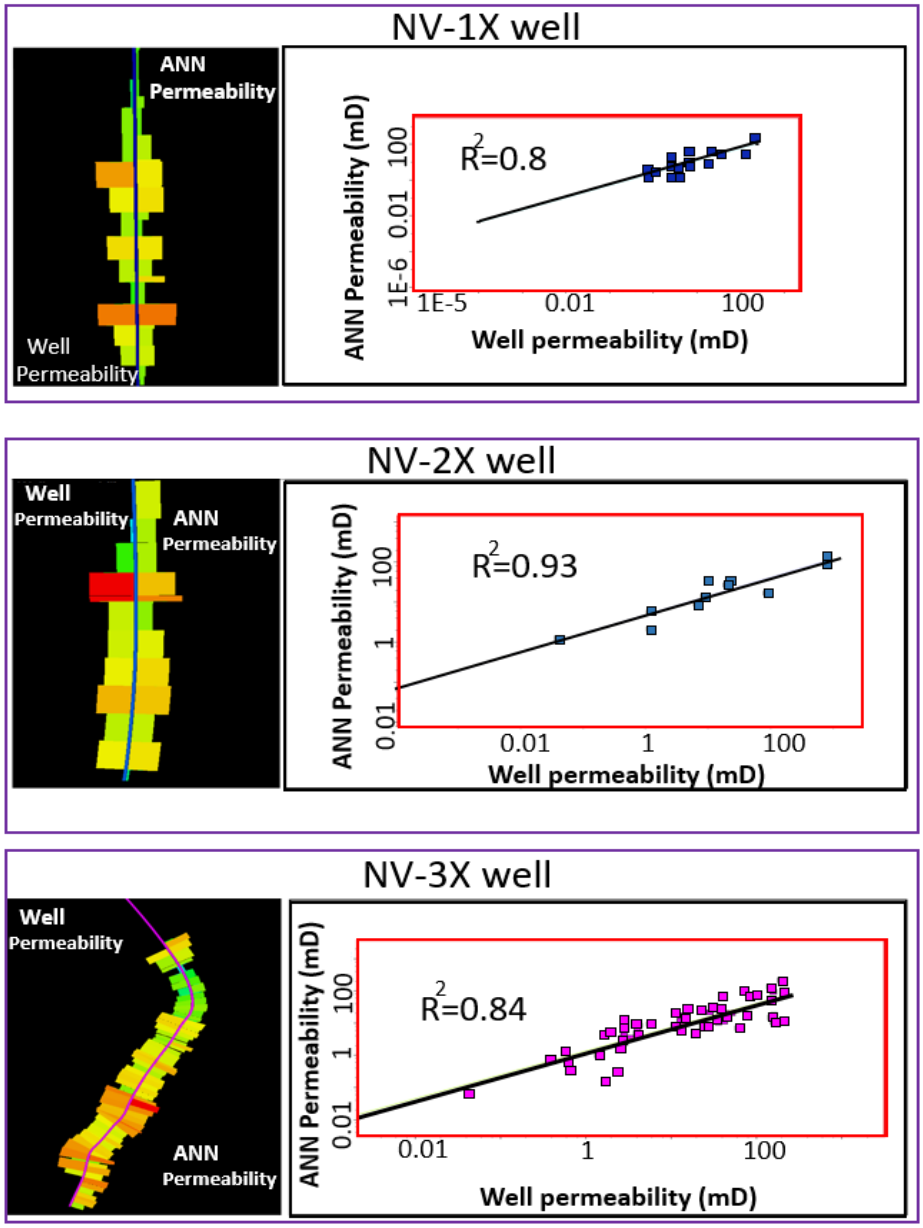

Figure 13. Cross-validation to check correlation factor between ANN and well log permeability values

3.4. POROSITY AND PERMEABILITY MODELING

The predicted porosity and permeability cubes as established by ANN was used as a reference to guide the porosity or permeability propagation in modeling based on the co-kriging technique. During the co-kriging process, it was aimed to combine well porosity with the predicted porosity cube to distribute in the 3D reservoir models. First, well porosity was upscaled and then modelled in petrophysical modeling by using SGS. Likewise, the predicted porosity cube is used as a secondary variable in collocated co-kriging.

A variogram was also important in the model trend. It was observed that, if the variogram range of major and minor directions is extremely large, then the well porosity tends to overrule the secondary variable and leads to a smooth picture of porosity along the horizontal axes. According to the conceptual geological model and FMI interpretation results, high porosity occurs in the vicinity of faults and drops away from faults. Thus, a large horizontal variogram was not applicable.

Consequently, two facies were established where the first facies included 2 wells, that is, NV-1X and NV-2X. The second facies had only one well, the NV-3X well. The range of the major direction of the first facies was set to 1,500 m and that of the minor direction was set to 1,000 m. The second facies was set to 1200 and 600 m, respectively. The dip was set in the main range from 65° to 85° based on FMI interpretation results and seismic data. This parameter was chosen to represent all azimuths of fractured zones, which is swept azimuth and compute co-kriging with step 15° following directions in a range from 45° to 90°. The final result of the co-kriging 3D porosity model was the average of the results of all the computed co-kriging processes.

The process of co-kriging is presented in **Figure 14,** and the porosity model is illustrated in **Figure 15a**. The co-kriging of the permeability model is similar to that of the porosity model. The well permeability was set as the primary variable. The 3D permeability model is presented in **Figure 15b**. The porosity and permeability models are used for further step to estimate the DST matching and CO_2 storage capacity in fractured basement reservoirs.

478

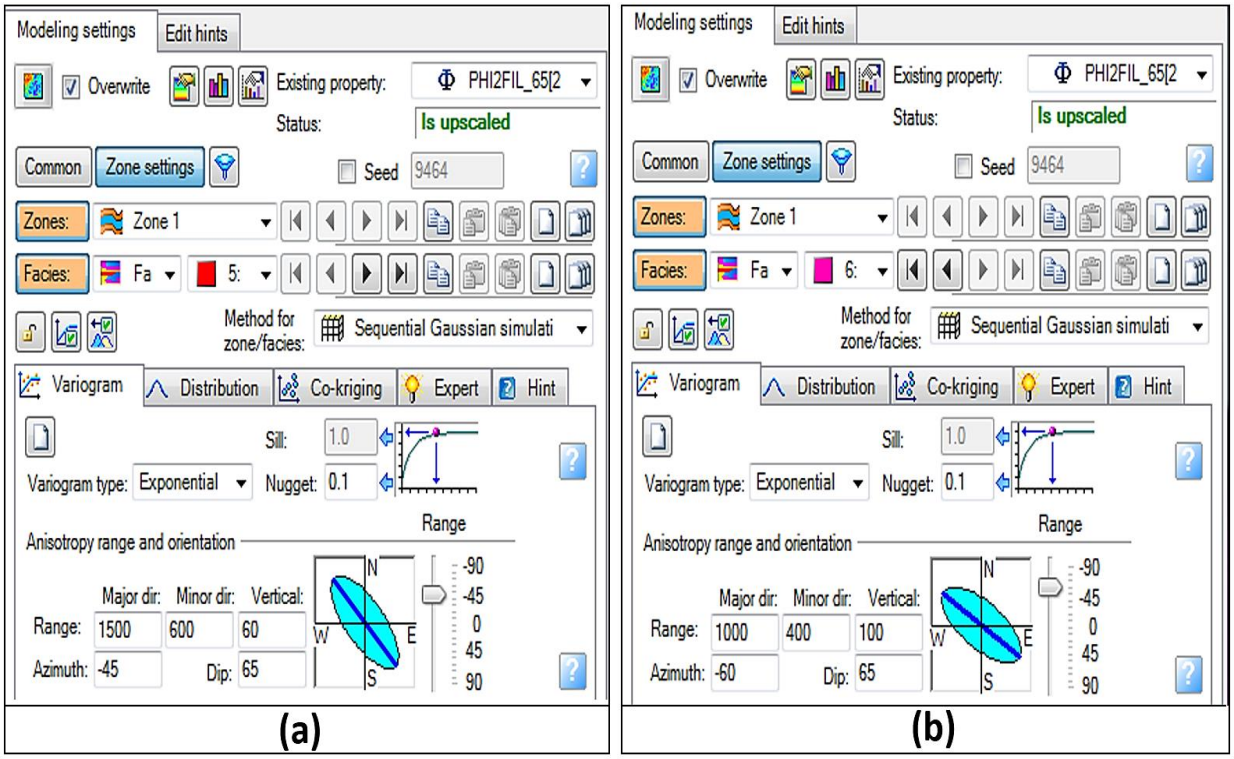

Figure 14. The co-kriging process to distribute porosity and permeability from integrated ANN and well log values. (a) Segment of NV-1X and NV-2X; (b) Segment of NV-3X

479

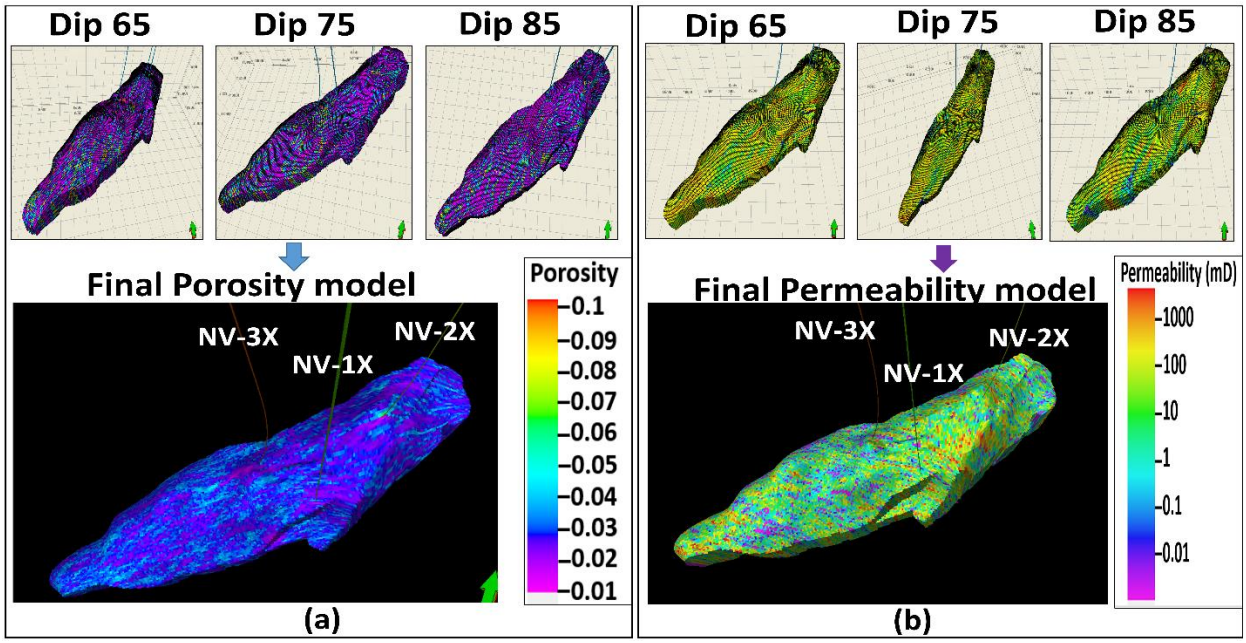

Figure 15. Co-kriging result to generate petrophysical model: (a) final porosity model and (b) final permeability model

3.5.RESERVOIR SIMULATION FOR DST MATCHING

3.5.1. Input data for reservoir simulation

A full field reservoir model was established using the result of geological modeling. A fine-scale grid size of 20 × 20 × 25 m cells were used without upscaling. The ECLIPSE 100 simulator (by Schlumberger) was used to construct a reservoir model. **Figure 16a** shows the 3D reservoir model consisting of 396,576 grids. This large grid system supports in serving the granite fractured basement with high accuracy.

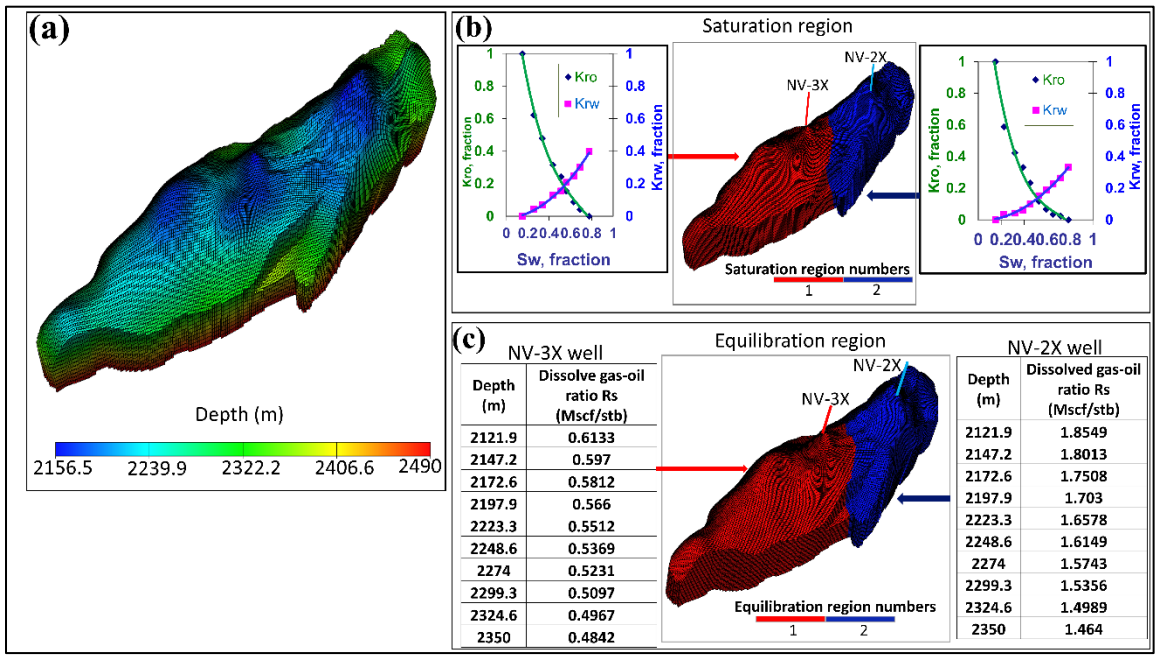

Figure 16. Preparation for DST matching: (a) reservoir model of dynamic simulation, (b) saturation region in fractured basement reservoirs, and (c) equilibration region in reservoir models

Aside from the static reservoir parameters used to populate the reservoir flow model from the geologic model, the latest available dynamic data, such as fluid contact, PVT, and SCAL, have also been included in this model. **Figure 16b** depicts the saturation region numbers, and the water-oil relative permeability curves used in the flow simulation model.

The reservoir simulation has been initialized with two PVT regions (i.e., equilibration regions). The first region covers the NV-3X well and the second covers the NV-2X well (**Figure 16c**). These areas are based on the differences in

oil properties as identified from the fluid sample. They are characterized by compositional gradients to be incorporated into the ECLIPSE 100 simulator by using a variation in dissolved gas–oil ratio with depth.

3.5.2. DST matching

The DST matching was conducted to determine the accuracy of geological models by comparing to the simulated values. In this study, two DSTs were used in the NV-2X and NV-3X wells to evaluate the reservoir characteristic. The model history matching has been applied to test data from these wells. The DST matching was conducted on the bottom-hole flowing pressure with the wells controlled by oil rate. The key parameter utilized in the match was permeability. Skin factors and fracture intersections in each well were used to determine the production index (PI) distribution along the well.

After the skin in each well was set to match the DST interpretation, the permeability was increased 2.5 times for the NV-3X well and decreased 0.3 times per NV-2X well. Moreover, a minor change to porosity around the NV-3X well (5% increase) is matched to the well-bottom hole pressure in the wells.

The co-kriging method was used to obtain the results. The final result of permeability and porosity after co-kriging is shown in **Figure 17.**

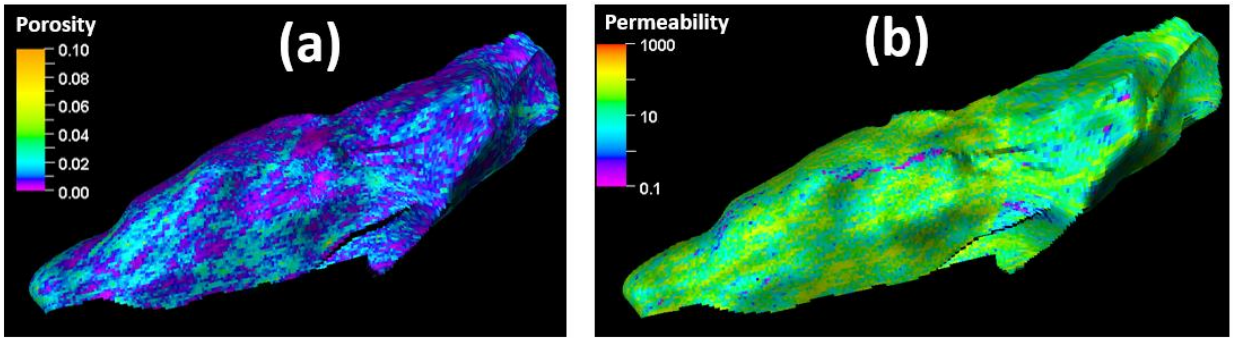

Figure 17. Reservoir geological model after DST matching: (a) porosity model and (b) permeability model

The DST matching is shown in **Figure 18**. The final skin and transmissibility (Kh) values after history matching in the model are compared with the DST interpretation in **Table 5**. The permeability shown in DST interpretations reflects the "outer" permeability of radial composite models that have been used in the DST

interpretations. The match between the model and DST interpretation is highly consistent in helping to improve confidence in the absolute permeability distribution of the model.

Table 5. The DST parameters after matching

Well	**NV-2X**		**NV-3X**	
	DST	Model	DST	Model
Skin (fraction)	2.7	2.7	-1.92	-1.92
Kh (mD.ft)	153089.00	162120.32	8191.57	8547.32

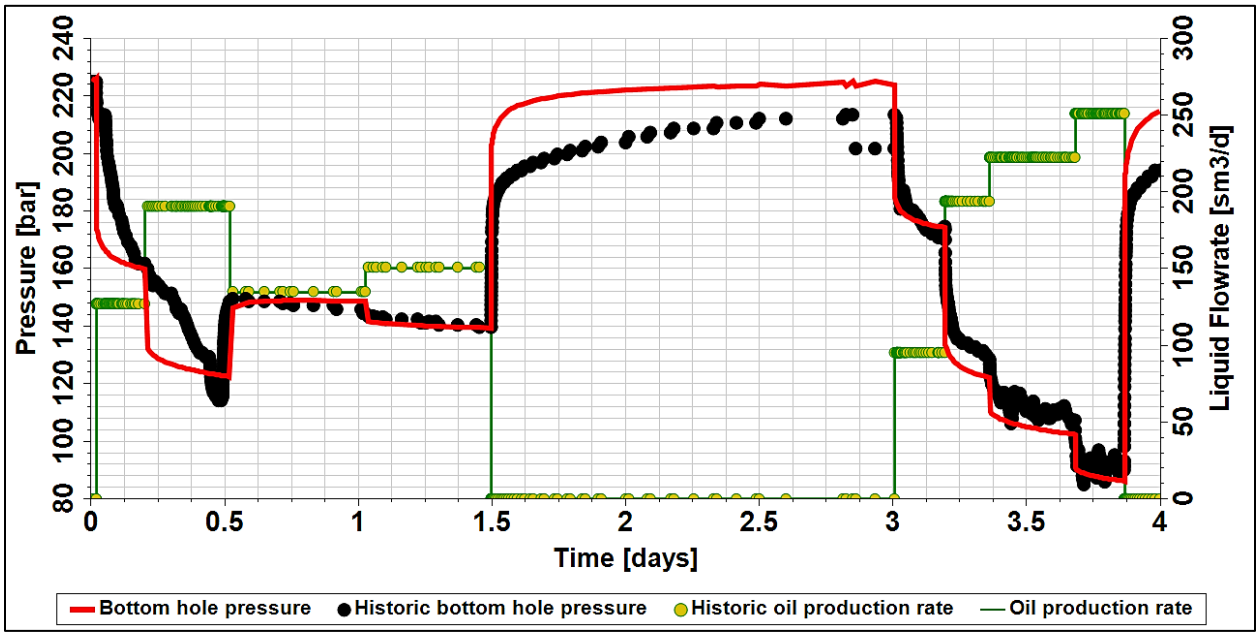

(a) NV-2X well DST matching

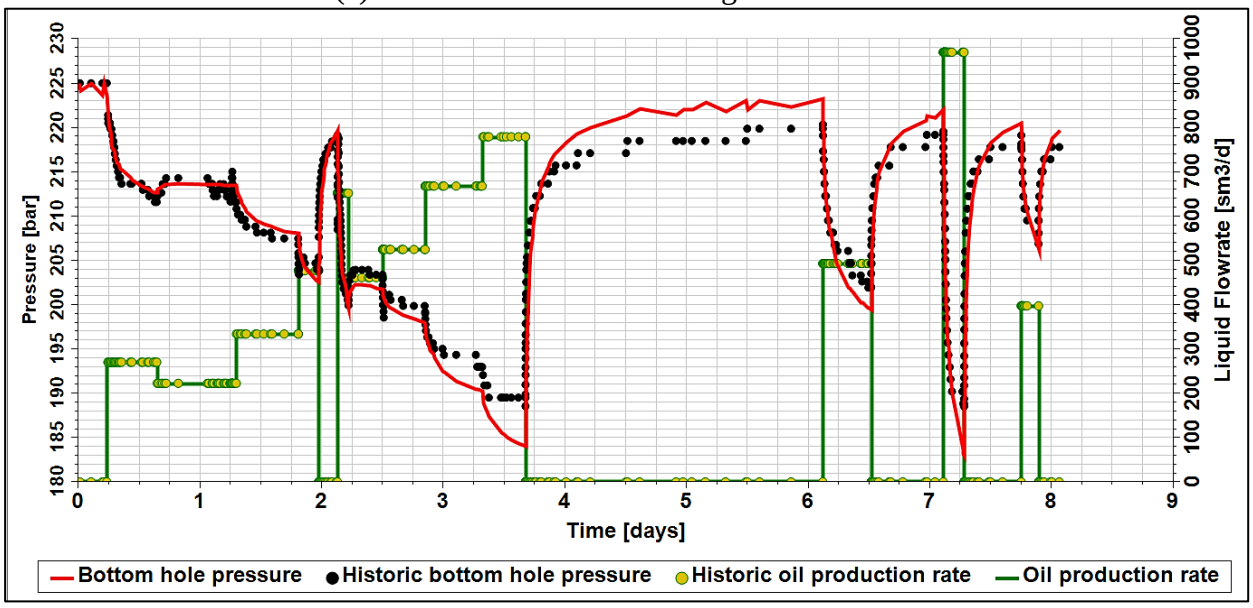

(b) NV-3X well DST matching

Figure 18. DST matching for fractured basement reservoirs

3.6. UNCERTAINTY ANALYSIS OF GEOLOGICAL MODEL

The DST matching evaluated the accuracy of the models through interactive responses between geological modeling and dynamic simulation. However, the following concerns remained in the geological model of granite fractured basement reservoirs:

- Geological parameters could not be obtained directly.
- Structural maps were still characterized by uncertainty due to seismic interpretation.
- Uncertainty remained in the co-kriging of facies models in the petrophysical model.
- Well, log and grid upscaling led to model uncertainty.

Therefore, geological uncertainty was necessary to perform the pore volume calculation. Thus, 200 cases were run for uncertainty analysis to determine the pore volume by modifying the variogram parameter in Petrel software. The Monte Carlo sampling method was applied to calculate the probability distribution of pore volume. The values of P10, P50, and P90 were subsequently adapted for risk analysis of the theoretical CO_2 storage capacity (**Figure 19**).

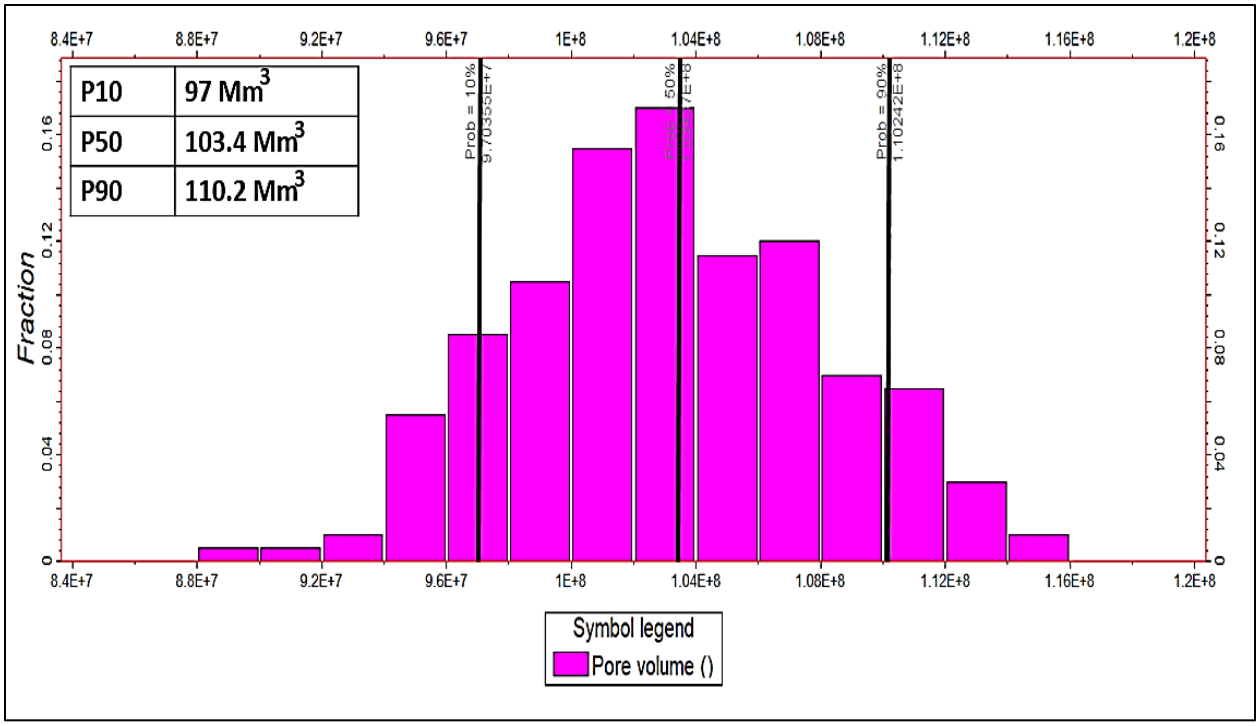

Figure 19. Geological uncertainty for theoretical CO_2 storage capacity

4. RESULT AND DISCUSSION

4.1.THEORETICAL CO_2 STORAGE CAPACITY

At this section, the main end goal of this study: theoretical CO2 Storage capacity is highlighted. This necessitated the reason for the in-depth elaboration of the above modeling methodology.

Several methods have been used to determine the CO_2 sequestration capacity for structural and stratigraphic trapping, residual gas trapping, as well as solubility trapping (Bradshaw et al., 2005). In this study, we focus on theoretical storage capacity in structural and stratigraphic trapping by using the following equation:

$$M_{CO2} = A \times h \times \Phi \times (1 - S_{wiir}) \times B \times \rho_{CO2} \times E\,, \quad (1)$$

where M_{CO2} is CO_2 storage mass (Mt), A is trap area (m^2), h is average thickness (m), Φ is porosity (%), S_{wiir} is irreducible water saturation (%), B is a formation volume factor (m^3/m^3), ρ_{CO2} is CO_2 density (kg/m^3), and E is the capacity coefficient that integrates trap heterogeneity, CO_2 sweep, and buoyancy efficiency (IEA GHG, 2008).

The CO_2 storage mass can be defined as an effective capacity by multiplying the storage effective coefficient C, which is trapping efficiency. The storage mass can be estimated based on the reservoir simulation. Trap area, porosity, and thickness can be evaluated accurately on 3D static geological modeling. Thus, instead of using **Eq. (1)**, we adapt summation of grid pore volumes ($V_{pv} = \sum_i A_i \times h_i \times \phi_i$) to replace $A \times h \times \Phi$, where A_i is model area, h_i is grid thickness and ϕ_i is the porosity of grid (Zhong and Carr, 2019). The new equation can be rewritten as follows:

$$M_{CO2} = V_{pv} \times (1 - S_{wiir}) \times B \times \rho_{CO2} \times E\,, \quad (2)$$

where V_{pv} is the total pore volume (m^3)

Therefore, the theoretical CO_2 storage capacity can be estimated by using **Eq. (2)** and **Table 6**. The least likely, P10, storage capacity was 7.02 million tons, and the most likely, P90, storage capacity was 99.5 million tons. In this light, we conclude that the fractured basement reservoir is capable of CO_2 storage due to the large amount of CO_2 that could be stored in the reservoir. However, the fractured basement is a complex reservoir for CO_2

injection. Thus, further investigation is necessary to improve the understanding of the CO_2 flow response in the reservoir.

Table 6. Uncertainty analysis for theoretical storage capacity in fracture basement reservoir

Parameters	Symbol	Unit	P10	P50	P90
Total pore volume	V_{pv}	Mm^3	97	103.4	110.2
Irreducible water saturation	S_{wiir}	%	0.35	0.25	0.1
Formation volume factor	B	Bbl/STB	1.45	1.45	1.45
Average CO_2 density	ρ_{CO2}	Kg/m^3	768.9	768.9	768.9
Capacity coefficient	E	%	0.1	0.5	0.9
CO_2 storage capacity	M_{CO2}	Mt	7.02	43.23	99.52

4.2. DISCUSSION

The presented workflow and results in this work show the complexity of constructing a 3D fractured basement type geological model. Nevertheless, the lack of adequate core and well log data makes this work quite challenging. Therefore, we constructed the 3D geological model integrating ANN, SGS and co-kriging based on the available data. Modeling results suggest that ANN is an efficient method in predicting porosity and permeability values. Also, utilizing SGS and co-kriging methodologies, the 3D model porosity and permeability were successfully distributed. Moreover, the workflow showed that DST matching is an important step to adjust the static geological model fitted with dynamic performance to improve the results of calculated theoretical CO_2 storage capacity. Lastly, the uncertainty quantification of theoretical capacity shows 7.02 to 99.52 million metric tons as a plausible range for potential CO_2-EOR and storage projects.

When using the ANN algorithm in 3D geological modeling workflow, ranking and selecting best scenario of the seismic attributes (Table 4) are the key factors to obtain the results with high correlation with well log data. This finding has a good agreement with other authors using the ANN approach for petrophysical modeling (Dang et al., 2015; Fang et al., 2017; Jalalalhosseini et al., 2014). However, these past studies paid no consideration to DST matching to investigate the reliability of the reservoir model in one single workflow. DST matching contributed toward validating the accuracy of porosity

and permeability through dynamic simulation. This step made the proposed method more unique to build a 3D geological model in fractured basement reservoir.

To conclude, our study proposes a useful workflow with limited core and well log data using ANN, SGS, co-kriging and DST matching. Due to the ease of application relative to the proposed workflow, it is recommended hitherto for other fractured basement reservoirs. A probable limitation to the proposed workflow is that the accuracy of geological models improves with the availability of more measurement data. Therefore, to investigate further, more data should be obtained and applied to this methodology. In addition, the calculation of the theoretical stored CO_2 only considered structural and stratigraphic trapping capacity. Thus, other CO_2 trappings, such as residual, dissolution, and mineral, should be performed to understand clearly the dynamics of CO_2 geo-sequestration in fractured basement reservoir.

5. CONCLUSIONS

Accurate estimation of static and dynamic CO_2 storage capacities in depleted oil reservoirs depends on the accuracy of permeability and porosity models. A reliable workflow for the construction of the 3D static geological model enhances the distribution of petrophysical properties. The workflow is useful to improve our understanding of CO_2/oil flow response during the CO_2 injection process to select optimal CO_2 storage locations. In many depleted oil and gas reservoirs, subsurface information, such as core, well logs, and accurate production history, are not always available.

ANN uses the available data to predict porosity and permeability with high correlation factor between predicted and measured values. The geostatistical method is integrated with ANN prediction to establish porosity and permeability distribution in fractured basement reservoirs. Co-kriging assigns the porosity and permeability of 3D models based on azimuth and dip parameters from FMI interpretation. The 3D porosity and permeability models could be used to investigate the fluid flow response and estimate the oil recovery factor as well as dynamic CO_2 storage capacity.

The following specific conclusions can be drawn from this study:

- Structural model construction is the first priority step for geological modeling.
- ANN is an effective method in predicting porosity and permeability based on seismic attributes and well log data.

- The ANN method can estimate porosity and permeability values with reasonable accuracy.
- Co-kriging simulation with suitable azimuth and dip parameters was integrated with ANN prediction values to establish the 3D petrophysical model in fractured basement reservoirs.
- Good DST matching indicated that the distribution of porosity and permeability is reliable in evaluating dynamic reservoir performance.
- Based on the calculations in Eq. (2), the P90–P10 theoretical CO_2 storage capacity ranges from 7.02 million tons to 99.5 million tons.

ACKNOWLEDGMENTS

The authors are grateful for the financial support provided by the ASEAN University Network Southeast Asia Engineering Education Development Network program and the Japanese International Cooperation Agency. We also thank Eric O. Ansah for his comments and discussion towards this manuscript

REFERENCES

ADB, 2012. Prospect for Carbon Capture and Storage in Southeast Asia. Asian Development Bank, Manilla. http://www.adb.org/publications/prospects-carbon- capture-and-storage-southeast-Asia (accessed 23 March 2019).

Ahmadi, M.A., 2015. Developing a Robust Surrogate Model of Chemical Flooding Based on the Artificial Neural Network for Enhanced Oil Recovery Implications. Math. Probl. Eng. 2015, 1–9. https://doi.org/10.1155/2015/706897

Ahmadi, M.A., 2011. Prediction of asphaltene precipitation using artificial neural network optimized by imperialist competitive algorithm. J. Pet. Explor. Prod. Technol. 1, 99–106. https://doi.org/10.1007/s13202-011-0013-7

Ahmadi, M.A., Ahmadi, A., 2016. Applying a sophisticated approach to predict CO2 solubility in brines: Application to CO2 sequestration. Int. J. Low-Carbon Technol. 11, 325–332. https://doi.org/10.1093/ijlct/ctu034

Ahmadi, M.A., Ahmadi, M.R., Hosseini, S.M., Ebadi, M., 2014a. Connectionist model predicts the porosity and permeability of petroleum reservoirs by means of petro-physical logs: Application of artificial intelligence. J. Pet. Sci. Eng. 123, 183–200. https://doi.org/10.1016/j.petrol.2014.08.026

Ahmadi, M.A., Ebadi, M., 2014. Evolving smart approach for determination dew point pressure through condensate gas reservoirs. Fuel 117, 1074–1084.

https://doi.org/10.1016/j.fuel.2013.10.010

Ahmadi, M.A., Ebadi, M., Marghmaleki, P.S., Fouladi, M.M., 2014b. Evolving predictive model to determine condensate-to-gas ratio in retrograded condensate gas reservoirs. Fuel 124, 241–257. https://doi.org/10.1016/j.fuel.2014.01.073

Ahmadi, M.A., Ebadi, M., Yazdanpanah, A., 2014c. Robust intelligent tool for estimating dew point pressure in retrograded condensate gas reservoirs: Application of particle swarm optimization. J. Pet. Sci. Eng. 123, 7–19. https://doi.org/10.1016/j.petrol.2014.05.023

Ahmadi, M.A., Shadizadeh, S.R., 2012. New approach for prediction of asphaltene precipitation due to natural depletion by using evolutionary algorithm concept. Fuel 102, 716–723. https://doi.org/10.1016/j.fuel.2012.05.050

Al-mudhafar, W.J., 2018. How is Multiple-Point Geostatistics of Lithofacies Modeling Assisting for Fast History Matching ? A Case Study from a Sand-Rich Fluvial Depositional Environment of Zubair Formation in South Rumaila Oil Field, in: Offshore Technology Conference. Houston, Texas, USA, 30 April–3 May 2018. This. https://doi.org/https://doi.org/10.4043/28662-MS

Ampomah, W., Balch, R., Will, R., Cather, M., Gunda, D., Dai, Z., 2017. Co-optimization of CO2-EOR and Storage Processes under Geological Uncertainty. Energy Procedia 114, 6928–6941. https://doi.org/10.1016/j.egypro.2017.03.1835

Anderson, D., McNeill, G., 1992. Artificial neural networks technology for neutron spectrometry and dosimetry, A DACS state-of-the-art report. https://doi.org/10.1093/rpd/ncm084

Bachu, S., 2018. Identification of oil reservoirs suitable for CO2-EOR and CO2 storage (CCUS) using reserves databases , with application to Alberta , Canada. Int. J. Greenh. Gas Control 44, 152–165. https://doi.org/10.1016/j.ijggc.2015.11.013

Bachu, S., 2008. CO2storage in geological media: Role, means, status and barriers to deployment. Prog. Energy Combust. Sci. 34, 254–273. https://doi.org/10.1016/j.pecs.2007.10.001

Bachu, S., 2002. Sequestration of CO2 in geological media in response to climate change: Road map for site selection using the transform of the geological space into the CO2 phase space. Energy Convers. Manag. 43, 87–102. https://doi.org/10.1016/S0196-8904(01)00009-7

Bachu, S., 2000. Sequestration of CO2 in geological media: Criteria and approach for site selection in response to climate change. Energy Convers. Manag. 41, 953–970. https://doi.org/10.1016/S0196-8904(99)00149-1

Bradshaw, J., Bachu, S., Bonijoly, D., Burruss, R., Christensen, N.P., Mathiassen, O.M., 2005. Task Force for Review and Identification of Standards, in: Carbon Sequestration Leadership Forum. Oviedo, Spain.

Bradshaw, J., Bachu, S., Bonijoly, D., Burruss, R., Holloway, S., Christensen, N.P., Mathiassen, O.M., 2007. CO2 storage capacity estimation: Issues and development of standards. Int. J. Greenh. Gas Control 1, 62–68. https://doi.org/10.1016/S1750-5836(07)00027-8

Choi, J.-W., Nicot, J.-P., Hosseini, S.A., Clift, S.J., Hovorka, S.D., 2013. CO2 recycling

711 accounting and EOR operation scheduling to assist in storage capacity assessment at a U.S.
712 gulf coast depleted reservoir. Int. J. Greenh. Gas Control 18, 474–484.
713 https://doi.org/10.1016/j.ijggc.2013.01.033

714 Cuong, T.X., Warren, J.K., 2009. Bach ho field, a fractured granitic basement reservoir, Cuu
715 Long Basin, offshore SE Vietnam: A "buried-hill" play. J. Pet. Geol. 32, 129–156.
716 https://doi.org/10.1111/j.1747-5457.2009.00440.x

717 Dai, Z., Zhang, Y., Stauffer, P., Xiao, T., Zhang, M., Ampomah, W., Yang, C., Zhou, Y., Ding,
718 M., Middleton, R., Soltanian, M.R., Bielicki, J.M., 2017. Injectivity Evaluation for Offshore
719 CO2Sequestration in Marine Sediments. Energy Procedia 114, 2921–2932.
720 https://doi.org/10.1016/j.egypro.2017.03.1420

721 Dang, C.T.Q., Chen, Z., Nguyen, N.T.B., Phung, T.H., 2015. An integrated geology and
722 reservoir engineering approach for modelling of a giant fractured basement reservoir. Int. J.
723 Oil, Gas Coal Technol. 10, 39–59. https://doi.org/10.1504/IJOGCT.2015.070043s

724 Darabi, H., Kavousi, A., Moraveji, M., Masihi, M., 2010. 3D fracture modeling in Parsi oil field
725 using artificial intelligence tools. J. Pet. Sci. Eng. 71, 67–76.
726 https://doi.org/10.1016/j.petrol.2010.01.004

727 Du, Y., W.W.Weiss, Xu, J., Balch, R.S., Li, D., 2003. SPE 84445 Obtain an Optimum Artificial
728 Neural Network Model for Reservoir Studies, in: SPE Annual Technical Conference and
729 Exhibition. Denver, Colorado, U.S.A,5 – 8 October.

730 Edwards, R.W.J., Celia, M.A., Bandilla, K.W., Doster, F., Kanno, C.M., 2015. A Model To
731 Estimate Carbon Dioxide Injectivity and Storage Capacity for Geological Sequestration in
732 Shale Gas Wells. Environ. Sci. Technol. 49, 9222–9229.
733 https://doi.org/10.1021/acs.est.5b01982

734 Esmaeilzadeh, S., Afshari, A., Motafakkerfard, R., 2013. Integrating artificial neural networks
735 technique and geostatistical approaches for 3D geological reservoir porosity modeling with
736 an example from one of Iran's oil fields. Pet. Sci. Technol. 31, 1175–1187.
737 https://doi.org/10.1080/10916466.2010.540617

738 Ettehadtavakkol, A., Lake, L.W., Bryant, S.L., 2014. CO2-EOR and storage design optimization.
739 Int. J. Greenh. Gas Control 25, 79–82. https://doi.org/10.1016/j.ijggc.2014.04.006

740 Fang, J., Zhou, F., Tang, Z., 2017. Discrete Fracture Network Modelling in a Naturally Fractured
741 Carbonate Reservoir in the Jingbei Oilfield, China. Energies 10.
742 https://doi.org/10.3390/en10020183

743 Ha-Duong, M., Nguyen-Trinh, H.A., 2017. Two scenarios for carbon capture and storage in
744 Vietnam. Energy Policy 110, 559–569. https://doi.org/10.1016/j.enpol.2017.08.040

745 Hill, B., Hovorka, S., Melzer, S., 2013. Geologic carbon storage through enhanced oil recovery.
746 Energy Procedia 37, 6808–6830. https://doi.org/10.1016/j.egypro.2013.06.614

747 Hitchon, B., Gunter, W.D., Gentzis, T., Bailey, R.T., 1999. Sedimentary basins and greenhouse
748 gases: A serendipitous association. Energy Convers. Manag. 40, 825–843.
749 https://doi.org/10.1016/S0196-8904(98)00146-0

750 Holloway, S., Savage, D., 1993. The potential for aquifer disposal of carbon dioxide in the UK.
751 Geotherm. Energy 34, 925–932.

752 Hung, N. Du, Le, H. Van, 2004. Petroleum Geology of Cuu Long Basin - Offshore Vietnam, in:
753 Proceedings of AAPG International Conference. Barcelona, Spain, September 21-24.

754 IEA GHG, I., 2008. Aquifer Storage-Development Issues.

755 Imai, N., Reeves, S., 2004. Feasibility study on CO2 EOR of white tiger field in Vietnam, in:
756 Third Annual DOE Conference on Carbon Capture and Sequestration. Alexandria, VA,
757 USA.

758 IPCC, 2005. IPCC special report on carbon dioxide capture and storage. Cambridge University
759 Press.

760 Iturrarán-Viveros, U., Parra, J.O., 2014. Artificial Neural Networks applied to estimate
761 permeability, porosity and intrinsic attenuation using seismic attributes and well-log data. J.
762 Appl. Geophys. 107, 45–54. https://doi.org/10.1016/j.jappgeo.2014.05.010

763 Jalalalhosseini, S.M., Ali, H., Mostafazadeh, M., 2014. Predicting porosity by using seismic
764 multi-attributes and well data and combining these available data by geostatistical methods
765 in a South Iranian oil field. Pet. Sci. Technol. 32, 29–37.
766 https://doi.org/10.1080/10916466.2011.584102

767 Kim, Y., Jang, H., Kim, J., Lee, J., 2017. Prediction of storage efficiency on CO2 sequestration
768 in deep saline aquifers using artificial neural network. Appl. Energy 185, 916–928.
769 https://doi.org/10.1016/j.apenergy.2016.10.012

770 Lee, E., Hornafius, J.S., Dean, E., Kazemi, H., 2019. Potential of Denver Basin oil fields to store
771 CO2 and produce Bio-CO2-EOR oil. Int. J. Greenh. Gas Control 81, 137–156.
772 https://doi.org/10.1016/j.ijggc.2018.11.013

773 Mahdavi, R., Kharrat, R., 2009. SPE 121214 Integration of 3D Seismic Attributes and Well Logs
774 for Electrofacies Mapping and Prediction of Reliable Petrophysical Properties.

775 Nguyen-Trinh, H.A., Ha-Duong, M., 2015. Perspective of CO2 capture & storage (CCS)
776 development in Vietnam: Results from expert interviews. Int. J. Greenh. Gas Control 37,
777 220–227. https://doi.org/10.1016/j.ijggc.2015.03.019

778 Nguyen, M.C., Zhang, Y., Li, J., Li, X., Bai, B., Wu, H., Wei, N., Stauffer, P.H., 2017. A
779 Geostatistical Study in Support of CO2Storage in Deep Saline Aquifers of the Shenhua
780 CCS Project, Ordos Basin, China. Energy Procedia 114, 5826–5835.
781 https://doi.org/10.1016/j.egypro.2017.03.1720

782 Nguyen, N.T., Dang, C.T.Q., Bae, W., 2011. Geological Characteristics and Integrated
783 Development Plan for Giant Naturally Fractured Basement Reservoirs. Can. Unconv.
784 Resour. Conf. 1–16. https://doi.org/10.2118/149510-MS

785 Nikravesh, M., 1998. Neural Network Knowledge-Based Modeling of Rock Properties Based on
786 Well Log Databases. SPE West. Reg. Meet. https://doi.org/10.2118/46206-ms

787 Pham, V., Halland, E., 2017. Perspective of CO2 for Storage and Enhanced Oil Recovery (EOR)

788 in Norwegian North Sea. Energy Procedia 114, 7042–7046.
789 https://doi.org/10.1016/j.egypro.2017.03.1845

790 Pyrcz, M.J., Deutsch, C. V., 2014. Geostastistical Reservoir Modeling. Oxford University Press,
791 Oxford.

792 Ruiz- Serna, M.A., Alzate- Espinosa, G.A., Obando- Montoya, A.F., Álvarez- Zapata, H.D.,
793 2019. Combined artificial intelligence modeling for production forecast in a petroleum
794 production field. CT&F - Ciencia, Tecnol. y Futur. 9, 27–35.
795 https://doi.org/10.29047/01225383.149

796 Schmidt, W.J., Hoang, B.H., Handschy, J.W., Hai, V.T., Cuong, T.X., Tung, N.T., 2019.
797 Tectonic evolution and regional setting of the Cuu Long Basin, Vietnam. Tectonophysics
798 757, 36–57. https://doi.org/10.1016/j.tecto.2019.03.001

799 Van't Veld, K., Mason, C.F., Leach, A., 2013. The economics of CO2sequestration through
800 enhanced oil recovery. Energy Procedia 37, 6909–6919.
801 https://doi.org/10.1016/j.egypro.2013.06.623

802 Vo Thanh, H., Sugai, Y., Sasaki, K., 2019. Impact of a new geological modelling method on the
803 enhancement of the CO 2 storage assessment of E sequence of Nam Vang field, offshore
804 Vietnam. Energy Sources, Part A Recover. Util. Environ. Eff. 41, 1–14.
805 https://doi.org/10.1080/15567036.2019.1604865

806 Wei, N., Li, X., Dahowski, R.T., Davidson, C.L., Liu, S., Zha, Y., 2015. Economic evaluation on
807 CO2-EOR of onshore oil fields in China. Int. J. Greenh. Gas Control 37, 170–181.
808 https://doi.org/10.1016/j.ijggc.2015.01.014

809 Zhao, X., Liao, X., 2012. Evaluation method of CO 2 sequestration and enhanced oil recovery in
810 an oil reservoir, as applied to the Changqing oilfields, China. Energy and Fuels 26, 5350–
811 5354. https://doi.org/10.1021/ef300783c

812 Zhong, Z., Carr, T.R., 2019. Geostatistical 3D geological model construction to estimate the
813 capacity of commercial scale injection and storage of CO2 in Jacksonburg-Stringtown oil
814 field, West Virginia, USA. nternational J. Greenh. Gas Control 80, 61–75.
815 https://doi.org/10.1016/j.ijggc.2018.10.011

816

817

818

819

820

821

822

823

Figure captions

Figure 1. Stratigraphic column of NV field in Cuu Long Basin.

Figure 2. NV field view showing a fractured basement reservoir as modelled in this study. The blue polygon indicates the study area. The red line shows distance from the CO_2 power plant to the injection site.

Figure 3. Illustration of data used in this study: (a) seismic horizon from seismic interpretation, (b) fault system in fractured basement reservoirs, (c) well log data including porosity and permeability values, and (d) FMI interpretation to obtain azimuth and dip parameters

Figure 4. Basic ANN structure. In this illustration, there are three input attributes, four neurons in the hidden layer, and two log samples in the output layer

Figure 5. Schematic representation of the integrated workflow to estimate theoretical CO_2 storage capacity

Figure 6. Upscaling porosity and permeability to define grid cell number for a structural model

Figure 7. Structural modeling process for fractured basement reservoirs. (a) Develop fault system; (b) skeleton grid; (c) final structural model

Figure 8. Seismic data for ANN training: (a) cross-section of seismic data along reservoir wells and (b) seismic attribute generation for the ANN process

Figure 9. Adoption of ANN structure to predict porosity values from upscale well log and seismic attributes: (a) structure of ANN model, (b) schematic of porosity prediction from ANN, and (c) correlation table of predicted and well log porosities

Figure 10. Distribution of porosity model from ANN

Figure 11. Cross-validation to check correlation factor between ANN and well log porosity values

Figure 12. Distributed permeability model as predicted by ANN

Figure 13. Cross-validation to check correlation factor between ANN and well log permeability values

Figure 14. The co-kriging process to distribute porosity and permeability from integrated ANN and well log values. (a) Segment of NV-1X and NV-2X; (b) Segment of NV-3X

Figure 15. Co-kriging result to generate petrophysical model: (a) final porosity model and (b) final permeability model

Figure 16. Preparation for DST matching: (a) reservoir model of dynamic simulation, (b) saturation region in fractured basement reservoirs, and (c) equilibration region in reservoir models

Figure 17. Reservoir geological model after DST matching: (a) porosity model and (b) permeability model

Figure 18. DST matching for fractured basement reservoirs

Figure 19. Geological uncertainty for theoretical CO_2 storage capacity